1	Managed aquifer recharge and exploitationextraction impacteffects on dynamics of					
2	groundwater level and quality <u>dynamics</u> in <u>a typical temperate semi-arid fissured karst</u>					
3	system northern China karst area: A multi-method quantitative study Quantitative					
4	research by multi-methods					
5						
6	Han Cao ^{1,2} , Jinlong Qian ^{1,2} , Huanliang Chen ^{3,4} , Chunwei Liu ^{3,4} , Shuai Gao ^{3,4} , Minghui Lyu ^{3,4} , Weihong					
7	Dong ^{1,2,*} , Caiping Hu ^{3,4,*}					
8						
9	¹ Key Laboratory of Groundwater Resources and Environments, Ministry of Education, Jilin University,					
10	Changchun, People's Republic of China					
1.1						
11	² Institute of Water Resources and Environment, Jilin University, Changchun, People's Republic of					
12	China					
12	China					
13	³ 801 Institute of Hydrogeology and Engineering Geology, Shandong Provincial Bureau of Geology &					
13	601 Institute of Hydrogeology and Engineering Geology, Shandong Hovincial Bureau of Geology &					
14	Mineral Resources, Jinan, China					
	Militar Resources, smail, emina					
15	⁴ Shandong Engineering Research Center for Environmental Protection and Remediation on					
16	Groundwater, Jinan, China					
17						
18	Corresponding Author: dongweihong@jlu.edu.cn, caipinghu126@126.com					
19						
20	Abstract					
21	Managed Aquifer Recharge (MAR) is an effective approach to mitigate groundwater decline and					
22	spring depletion in karst systems impacted by excessive exploitation. However, the hydrogeological					
22						
23	complexity of karst aquifers makes groundwater quantity and quality highly sensitive to human activities,					
24	and a delinear for MAD instrumental of This wide devilor on the state of the					
24	posing challenges for MAR implementation. This study develops an integrated multi-method					
25	framework—combining isotopic analysis, flow monitoring, tracer tests, and numerical modeling—to					
23	1					

evaluate the effects of MAR and groundwater extraction on karst aquifer dynamics, with a case study in the Baotu Spring system (Jinan, China). To enhance the accuracy of recharge rate quantification, an $\underline{enhanced\ isotope\ mixing\ model\ that\ reduces\ uncertainties\ in\ estimating\ groundwater\ recharge\ ratios\ from}$ multiple sources was developed, and the MAR rate settings were refined by establishing a quantitative relationship between effective MAR rates and water release rates through river flow monitoring. To improve the solute transport simulations reliability, we conducted field tracer tests to constrain the effective porosity of the karst aquifer - a parameter typically poorly constrained in such systems. Furthermore, we validated the applicability of the equivalent porous media (EPM) model through rigorous hydrodynamic analysis, using field-measured fracture apertures to calculate Reynolds numbers and verify laminar flow conditions. The results demonstrate that surface water contributes >80% of recharge near MAR implementation zones, with MAR efficiency decreasing beyond critical river discharge thresholds. The karst aquifer exhibits laminar flow (effective porosity = 1.08×10⁻⁴), confirming the validity of the EPM approach. Modeling reveals that MAR significantly raises water tables, though efficiency varies by different MAR sources, and MAR-induced sulfate concentrations must be maintained below 56.5, 197.8, and 339.1 mg/L to meet China's Class I, II, and III groundwater standards, respectively. These findings provide practical guidelines for MAR implementation in temperate semiarid fissured karst systems. Managed aquifer recharge (MAR) is an effective way to counter groundwater level decline and spring depletion caused by excessive groundwater exploitation in karst areas. However, the unique characteristics of karst groundwater systems make the groundwater quantity and quality more susceptible to human activities, posing challenges for MAR research. This research employed multi-methods including numerical simulations, isotope analysis, infiltration tests, flow monitoring and tracer tests to

26

27

28

29

30

31

32

33

34

35

36

37

38

39

40

41

42

43

44

45

46

quantitatively analyze the impacts of MAR and groundwater exploitation on the dynamics of groundwater level and quality in a typical northern China karst area, the Baotu Spring area in Jinan City. First, the percentage of surface water recharge in karst groundwater was calculated using isotope data with the improved two-end-member mixing model. Next, the quantitative relationship between volume of released water and actual recharge was established with data from infiltration tests and flow monitoring. Then, the actual groundwater flow velocity and effective porosity of the karst aquifers were calculated with former tracer test isochrone maps. Finally, the impacts of MAR and groundwater exploitation on dynamics of groundwater level and quality were quantitatively analyzed with a groundwater flow-solute transport model for the area. The results indicate that the MAR and groundwater exploitation in the Baotu Spring area have significantly impacted karst groundwater levels and quality. These complementary methods enhance the accuracy of decisions in MAR and groundwater exploitation.

Keywords: Managed aquifer recharge (MAR); Temperate semi-arid regionKarst groundwater; Fissured karst Quantitative analysis; Multi-methods.

1. Introduction

Managed aquifer recharge (MAR) (Sherif et al., 2023), refers to the intentional recharge of aquifers to address the ecological and environmental geological issues caused by excessive groundwater exploitation (Aeschbach-Hertig & Gleeson, 2012; Foley et al., 2011). It has been demonstrated that appropriate recharge can effectively elevate groundwater levels and improve groundwater quality to some extent (Ajjur & Baalousha, 2021; Alam et al., 2021; Standen et al., 2020).

Karst groundwater constitutes a vital water resource (Hartmann et al., 2014; Medici et al., 2021), with managed aquifer recharge (MAR) in karst systems emerging as a key research focus (Zhang & Wang, 2021). Unlike pore water, karst groundwater is stored in dissolution conduits and fissures,

exhibiting high heterogeneity, rapid flow velocities, and concentrated discharge. These properties increase the susceptibility of karst aquifers to anthropogenic impacts on both quantity and quality (Allocca et al., 2014; Lorenzi et al., 2024), complicating MAR implementation. The extreme heterogeneity of karst systems results in spatially variable MAR effectiveness (Daher et al., 2011), with recharge impacts on groundwater levels and quality differing by water source. Rapid flow dynamics (Bakalowicz, 2005) lead to extensive well catchment areas, where over-exploitation can induce largescale drawdown cones and associated geological risks (Jiang et al., 2019). Furthermore, MAR using contaminated source water may accelerate pollutant transport (H. Cao et al., 2023), jeopardizing groundwater quality (Xanke et al., 2017). Thus, quantitative assessment of MAR and extraction effects on karst groundwater is critical for ensuring sustainable and safe aquifer management. Karst groundwater is a crucial component of water resources (Hartmann et al., 2014; Medici et al., 2021). The research of MAR in karst areas has become a prominent focus in recent years (Zhang & Wang, 2021). However, the unique characteristics of karst groundwater systems make the groundwater quantity and quality more susceptible to human activities (Allocca et al., 2014; Lorenzi et al., 2024), posing challenges for MAR research. Due to the highly heterogeneous nature of karst development, the actual effectiveness of MAR varies significantly across different locations (Daher et al., 2011). The impact of recharge on the karst groundwater level and quality at different locations and using various water sources shows significant variation. Additionally, the fast karst groundwater flow (Bakalowicz, 2005) leads to extensive catchment areas for karst groundwater exploitation wells, and over-exploitation would create large-scale groundwater level drawdown cones, causing secondary geological hazards (Jiang et al., 2019). Moreover, if poor-quality source water were used for MAR, pollutants would quickly spread downstream (H. Cao et al., 2023), severely threatening the quality of karst groundwater (Xanke

70

71

72

73

74

75

76

77

78

79

80

81

82

83

84

85

86

87

88

89

90

et al., 2017). Therefore, quantitatively assessing the effects of MAR and groundwater exploitation on the quantity and quality of karst groundwater will facilitate stable, efficient, and safe aquifer recharge and groundwater exploitation. From a global perspective, significant differences exist in karst development and groundwater flow characteristics among different countries and regions. The Baotu Spring karst aquifer in Jinan, China, representing the fissured karst system in the temperate semi-arid region, exhibits remarkable hydrogeological representativeness worldwide (Liang et al., 2018). In these areas, karst aquifers typically develop in Cambrian-Ordovician carbonate formations, with their hydrogeological features being strongly controlled by geological structures. The primary aquifer medium consists of karst fissures formed by well-developed tectonic fissures, ultimately giving rise to a groundwater system dominated by an extensive network of karst fissures (Aliouache & Jourde, 2024; Jiang et al., 2022). In temperate semi-arid regions, the persistent development of dissolution is constrained by the low permeability of soluble rocks (dominated by fracture flow) and limited hydrothermal conditions, resulting in the prolonged stagnation of underground karst systems at the fracture network stage and hindering their evolution into large-scale cave or conduit systems. Moreover, such regions often feature large karst springs as concentrated discharge points of groundwater (Criss, 2010). Due to seasonal recharge fluctuations (primarily from precipitation) (Bhering et al., 2021), these springs exhibit significant discharge variations. Therefore, scientifically adjusting recharge strategies based on precipitation variability to maintain spring flow constitutes a key research issue. In China, temperate semi-arid fissured karst groundwater systems similar to the Baotu Spring are predominantly distributed across several northern provinces, including Shandong (Liu et al., 2021), Shanxi (Zhang et al., 2018), Hebei (M. Gao et al., 2023), Henan (Yin et al., 2023) and Shaanxi (Li et al.,

92

93

94

95

96

97

98

99

100

101

102

103

104

105

106

107

108

109

110

111

112

2020). Globally, systems exhibiting varying degrees of similarity can be observed in certain regions, notably in the U.K (Agbotui et al., 2020), France (Ballesteros et al., 2020), Germany (Knöll & Scheytt, 2017), Italy (Pagnozzi et al., 2020), the U.S (Criss, 2010) and Canada (Perrin et al., 2011). These regions all face similar challenges related to seasonal drought and karst groundwater pollution. The research on karst groundwater at Baotu Spring and its artificial recharge practices can provide valuable insights for these areas. Existing research on the effects of managed aquifer recharge (MAR) and extraction on groundwater level and quality has established relatively mature methodologies (Ringleb et al., 2016). However, most approaches remain qualitative or semi-quantitative. Hydrogeochemical and isotopic techniques are widely employed in MAR studies (Akurugu et al., 2022; M. Li et al., 2023). Isotopic tracers are frequently used to identify recharge sources, and the integration of multiple hydrochemical and isotopic indicators (Guo et al., 2019) allows estimation of source contributions (Deng et al., 2022). Nevertheless, this method faces challenges, including the inherent non-uniqueness of solutions and uncertainty in determining precise isotopic signatures for individual recharge source, which may compromise accuracy. Additionally, the scarcity of long-term isotopic monitoring data restricts the applicability of this approach for analyzing temporal variations in MAR effects. There are some relatively mature research methods regarding the effects of MAR and groundwater exploitation on groundwater level and quality (Ringleb et al., 2016). However, most of these methods are either qualitative or semi-quantitative. Hydrogeochemical and isotope methods are commonly used in MAR studies (Akurugu et al., 2022; M. Li et al., 2023). By monitoring the changes in groundwater quality before and after the recharge, the impact of MAR on groundwater quality can be qualitatively analyzed. A primary issue with hydrogeochemical analysis is that its conclusions may be ambiguous, as

114

115

116

117

118

119

120

121

122

123

124

125

126

127

128

129

130

131

132

133

134

potential unknown sources of groundwater contamination could interfere with the results. In addition, isotopes in groundwater are often used to identify recharge sources. By combining multiple hydrochemical and isotopic indicators (Guo et al., 2019), the proportion of various recharge sources contributing to groundwater can be estimated (Deng et al., 2022). However, in many cases, due to the inability to accurately determine the isotopic values for each recharge source, this method can only provide a rough estimate. Furthermore, due to the typical lack of long-term monitoring data on groundwater isotopes, this approach is unsuitable for studying the dynamics in the effects of MAR on groundwater. Numerical simulation serves as an effective method for MAR quantitative analysis (Medici et al., 2021; Ostad-Ali-Askari & Shayannejad, 2021; Zafarmomen et al., 2024). The selection of simulation programs depends on karst aquifer characteristics. While conduit flow process (CFP) models are suitable for well-developed karst systems (Chang et al., 2015), their application is constrained by the requirement for detailed conduit dimension data, particularly in regional-scale modeling (Jourde & Wang, 2023). Numerical simulation is a powerful tool for quantitative research of MAR (Medici et al., 2021; Ostad-Ali-Askari & Shayannejad, 2021; Zafarmomen et al., 2024). Previous studies have demonstrated the feasibility of employing a simplified equivalent porous medium (EPM) model without embedded karst conduits for regional groundwater numerical simulations in temperate semi-arid fissured karst systems with limited karst development (Kang et al., 2011; Luo et al., 2020; Scanlon et al., 2003). However, these studies often lack field investigations to verify whether groundwater flow regimes satisfy the laminar flow assumption inherent to EPM models (Agbotui et al., 2020; Medici et al., 2024). The Equivalent Porous Medium (EPM) model, represented by MODFLOW, is suitable for simulating laminar

136

137

138

139

140

141

142

143

144

145

146

147

148

149

150

151

152

153

154

155

156

157

groundwater flow that adheres to Darcy's law (Jourde & Wang, 2023; Ringleb et al., 2016). In karst

regions with low development, such as the karst areas in northern China, groundwater flow is predominantly laminar, largely complying with Darcy's law. Therefore, the EPM model without inserting karst-conduits embedded is well-suited for application in these regions. When conducting MAR studies using numerical simulation methods, accurately determining the actual groundwater recharge rate is a crucial condition for ensuring the accuracy of the simulation results. In the studies of MAR primarily driven by riverbed infiltration, methods such as riverbed infiltration tests and river flow monitoring can be employed. By applying the principles of groundwater dynamics and water balance, the actual surface water recharge to groundwater can be quantitatively calculated. Studies indicate that accurate estimation of effective porosity in karst aquifers is critical when simulating solute transport using the equivalent porous medium (EPM) model (Kidmose et al., 2023; Ren et al., 2018). Overestimation of effective porosity often leads to underestimated groundwater flow velocities, introducing significant errors in pollution control strategies (Medici & West, 2021; Medici et al., 2019). To improve EPM model reliability, effective porosity should be derived from regional-scale hydraulic tests (e.g., tracer test) (Medici & West, 2021; Worthington et al., 2019; Zhu et al., 2020). Similarly, in MAR studies using numerical simulations, precise determination of groundwater recharge rates is essential for result accuracy (Hartmann et al., 2015). For MAR driven by riverbed infiltration, methods such as infiltration tests (Xi et al., 2015) and riverflow monitoring can quantify recharge rates via hydrodynamics and water-balance principles. Cross-validation of these methods in field studies reduces uncertainty from data limitations, enhancing MAR-related quantitative assessments (Mudarra et al., 2019). Furthermore, it has been indicated that when using the EPM model for simulating solute transport in karst groundwater, properly estimating the effective porosity of karst aquifers is

158

159

160

161

162

163

164

165

166

167

168

169

170

171

172

173

174

175

176

177

178

179

critically important (Kidmose et al., 2023; Ren et al., 2018). Overestimating the effective porosity often

results in a severe underestimation of the actual groundwater velocity, leading to significant errors in karst groundwater pollution control measures (Medici & West, 2021; Medici et al., 2019). Therefore, to ensure the effective application of the EPM model in groundwater solute transport simulating, it is advisable to consider estimating the effective porosity of the karst aquifer medium using the actual groundwater flow velocity calculated from tracer tests (Medici & West, 2021; Worthington et al., 2019; Zhu et al., 2020).(Hartmann et al., 2015)(Xi et al., 2015) In MAR studies conducted in actual regions, the results of various methods mentioned above can be cross-validated to reduce the uncertainty caused by data searcity or insufficient investigation, thereby improving the accuracy of quantitative research related to MAR (Mudarra et al., 2019). The Baotu Spring area in Jinan City is a typical representative of the karst areas in northern China (Liang et al., 2018), with karst groundwater serving as one of the crucial water supply sources. In the decades, the increasing demand for water resources in Jinan has led to excessive groundwater exploitation, causing a decline in groundwater levels and the drying up of springs. In order to balance the needs of water supply and spring protection, Jinan City has implemented the project of MAR using the diverted water from the Yellow River (Kang et al., 2011) and the Yangtze River from the South-to-North Water Transfer Project in recent years. Studies have shown that there is a close hydraulic connection between surface water and karst groundwater in certain of the Yufu River and Xingji River, making them ideal sites for implementing the MAR project (J. Li et al., 2023). However, when the flow of Yufu River is excessively high, a portion of the flow downstream and cannot recharge the karst groundwater. Moreover, the concentration of some hydrochemical components in the diverted water may be higher than those of the local karst groundwater—and thus long-term use of lower-quality water for

180

181

182

183

184

185

186

187

188

189

190

191

192

193

194

195

196

197

198

199

200

201

recharge may lead to continuous deterioration of karst groundwater quality.

This study proposes an integrated multi-method analytical approach to quantitatively assess the effects of managed aquifer recharge (MAR) and extraction on groundwater levels and quality in temperate semi-arid fractured karst systems. The approach combines coupled numerical modeling of groundwater flow and solute transport with supplementary techniques—isotope analysis, infiltration tests, flow monitoring, and tracer tests—to improve simulation accuracy. Using Jinan's Baotu Spring karst aquifer as a case study, we evaluate how MAR and extraction influence karst groundwater dynamics, aiming to ensure stable regional water levels, long-term water quality security, and sustainable groundwater resource utilization. Therefore, to ensure the stability of the karst groundwater level and the long-term safety of water quality, and to guarantee the sustainable exploitation of groundwater resources, the purpose of this research is to quantitatively analyze the impacts of MAR and groundwater exploitation on the dynamics of karst groundwater level and quality in the Baotu Spring area of Jinan City by multimethods. The method employed in this study primarily focuses on the numerical simulation of coupled groundwater flow and solute transport. Complementary techniques such as isotope analysis, infiltration tests, flow monitoring, and tracer tests are also utilized to enhance the accuracy of the numerical simulations. The specific objectives of this research are as follow: (1) To determine the sources of groundwater recharge and quantify the mixing ratios and spatial distribution of recharge using multisource data. (2) To quantify the effective infiltration recharge of the MAR segments under varying water release rates for groundwater flow modeling inputs. (3) To estimate the effective porosity of aquifers as a key parameter for groundwater solute transport modeling. (4) To establish a groundwater flow-solute transport model for the study area based on the validated the EPM model's applicability, and to quantitatively evaluate the impacts of MAR and extraction on groundwater level and quality dynamics.

2. Material and Methods

202

203

204

205

206

207

208

209

210

211

212

213

214

215

216

217

218

219

220

221

222

2.1. Study area

116°50'0"E

116°50'0"E

224

225

226

227

228

229

230

231

232

233

The study area of this paper is the Baotu Spring area, located in Jinan City, Shandong Province, China, covering about 1,654 km² (Niu et al., 2021) (Fig. 1). The terrain of Baotu Spring area is higher in the south and lower in the north, featuringwith rolling steep mountains and deep canyons in the south, low mountains and hills in the middle, and Piedmont inclined plains and alluvial plains in the north. The Baotu Spring area is located in the mid-latitude inland area with a warm temperate continental climate. The average annual precipitation from 1951 to 2024 is 690.4 mm, mostly falling between June and September (accounting for 77% of the total), and southern mountainous areas receive more precipitation than northern plains.

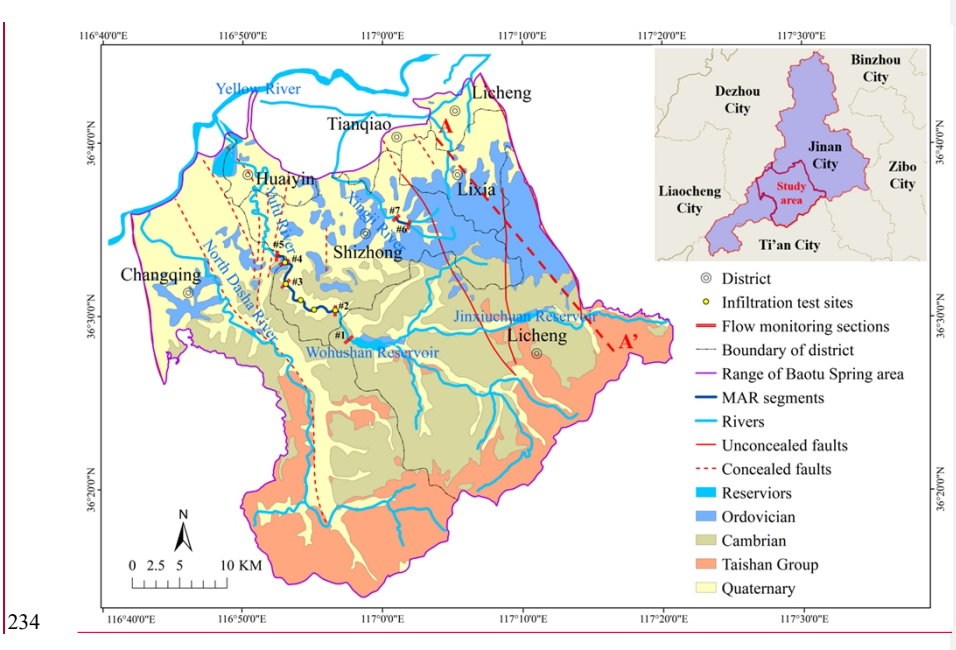
Tianqiao Tianqiao Likid Liacheng City Ti'an City Changqing City City

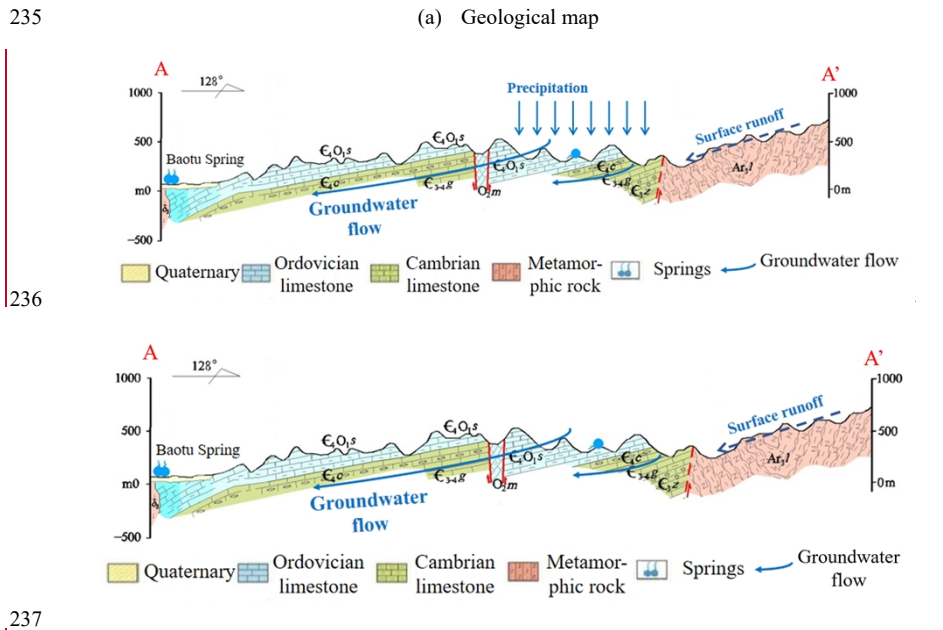
117°30'0"E

Rivers
Reserviors
Ordovician strata
Cambrian strata
Metamorphic rock
Quaternary strata

117°20'0"E

117°10'0"E





(b) Hydrogeological cross-sectionprofile

238

239

240

Fig._1 Geological map and hydrogeological cross-sectionprofile of Baotu Spring area

The main rivers in this region are the Yellow River, Yufu River, Xingji River, and North Dasha

River (Fig1). The Yellow River forms the study area's northwestern boundary and is mainly used for						
agricultural irrigation and groundwater recharge. The Yufu River is a seasonal tributary of the Yellow						
River, and the segments between Zhaiertou and Cuima Villages has excellent permeability, making it an						
ideal river for MAR (Guo et al., 2019) (Fig. 5(b)). Additionally, the Xingji River in the northeast, though						
small, also has a permeable riverbed making it suitable for MAR (Fig5(b)).						
Geologically, the study area is characterized by a northward-dipping monocline predominantly						
composed of Paleozoic carbonate rock layers. Several large-scale NNW-trending faults are						
developed within this area. Except for the Dongwu Fault and Mashan Fault forming the eastern and						
western boundaries of the study area, respectively, the other faults are generally permeable. The						
stratigraphic units exposed in the study area from south to north, listed from oldest to youngest, are as						
follows: Archaean Taishan Group metamorphic rocks, Cambrian limestone, Ordovician limestone, and						
Quaternary loose sediments (Fig1)						
Quaternary loose sediments (Fig1) The eExploitable karst groundwater is stored in the Zhangxia Formation of the middle Cambrian,						
The eExploitable karst groundwater is stored in the Zhangxia Formation of the middle Cambrian,						
The eExploitable karst groundwater is stored in the Zhangxia Formation of the middle Cambrian, the Chaomidian Formation of the upper Cambrian, and the Majiagou Formation of the Ordovician. In						
The eExploitable karst groundwater is stored in the Zhangxia Formation of the middle Cambrian, the Chaomidian Formation of the upper Cambrian, and the Majiagou Formation of the Ordovician. In the northern mountainous and hilly areas, karst groundwater is recharged by precipitation and surface						
The eExploitable karst groundwater is stored in the Zhangxia Formation of the middle Cambrian, the Chaomidian Formation of the upper Cambrian, and the Majiagou Formation of the Ordovician. In the northern mountainous and hilly areas, karst groundwater is recharged by precipitation and surface water, flowing northward along strata dips (Zhu et al., 2020). In the northern piedmont alluvial plain, the						
The eExploitable karst groundwater is stored in the Zhangxia Formation of the middle Cambrian, the Chaomidian Formation of the upper Cambrian, and the Majiagou Formation of the Ordovician. In the northern mountainous and hilly areas, karst groundwater is recharged by precipitation and surface water, flowing northward along strata dips (Zhu et al., 2020). In the northern piedmont alluvial plain, the karst aquifer is buried under Quaternary sediments. Late Mesozoic Llarge gabbro intrusions from the late						
The eExploitable karst groundwater is stored in the Zhangxia Formation of the middle Cambrian, the Chaomidian Formation of the upper Cambrian, and the Majiagou Formation of the Ordovician. In the northern mountainous and hilly areas, karst groundwater is recharged by precipitation and surface water, flowing northward along strata dips (Zhu et al., 2020). In the northern piedmont alluvial plain, the karst aquifer is buried under Quaternary sediments. Late Mesozoic Llarge gabbro intrusions from the late Mesozoic block the northward flow, causing the water to rise along fracture fissures and form springs						
The eExploitable karst groundwater is stored in the Zhangxia Formation of the middle Cambrian, the Chaomidian Formation of the upper Cambrian, and the Majiagou Formation of the Ordovician. In the northern mountainous and hilly areas, karst groundwater is recharged by precipitation and surface water, flowing northward along strata dips (Zhu et al., 2020). In the northern piedmont alluvial plain, the karst aquifer is buried under Quaternary sediments. Late Mesozoic Llarge gabbro intrusions from the late Mesozoic block the northward flow, causing the water to rise along fracture fissures and form springs (Niu et al., 2021; Wang et al., 2022), with Baotu Spring being the most popular of them (Guo et al.,						

past decades, the increasing demand for water resources in Jinan has led to excessive groundwater exploitation, causing a decline in groundwater levels and the drying up of springsAs a crucial water supply source for Jinan, decades of increasing demand for groundwater have led to over-exploitation, causing water level decline and spring drying (S. Gao et al., 2023). In order (To balance the needs of water supply and spring protection, Jinan City has implemented the project of MAR projects using the diverted water from the Yellow River (Kang et al., 2011) and the Yangtze River from the South-to-North Water Transfer Project (Liu et al., 2020) in recent years. Studies have shown that there is a close hydraulie connection between surface water and karst groundwater in certain_segments_of the Yufu River and Xingji River, making them ideal sites for implementing the MAR project (J. Li et al., 2023). Most MAR occurs along segments of the Yufu and Xingji Rivers, with minor MAR through dedicated wells in urban areas (which are no longer used for extraction) (Wang et al., 2017). Notably, excessive flow in the Yufu River may bypass recharge zones, and some diverted water components (e.g., hydrochemical concentrations) may exceed local karst groundwater standards (X. Cao et al., 2023; J. Li et al., 2023; Zheng et al., 2020), posing risks of long-term quality deterioration (J. Li et al., 2023; Zhang & Wang, 2021). Currently, few groundwater exploiting wells remain active, categorized into three groups by location: western suburbs, western Jinan, and eastern suburbs wells. All exploiting wells, MAR wells, and MAR river segments are mapped in Fig. 5(b). However, when the flow of Yufu River is excessively high, a portion of the flow downstream and cannot recharge the karst groundwater. Moreover, the concentration of some hydrochemical components in the diverted water may be higher than those of the local karst groundwater, and thus long term use of lower-quality water for recharge may lead to continuous deterioration of karst groundwater quality. In addition, only few of the groundwater exploiting wells in the study area are still under exploitation, which could be categorized into three

263

264

265

266

267

268

269

270

271

272

273

274

275

276

277

278

279

280

281

282

283

groups (western suburbs wells, western Jinan wells and eastern suburbs wells) based on the locations.

Most of the MAR in the study area is conducted along certain river segments of the Yufu River and

Xingji River, while a small portion of the MAR is carried out through specific wells in the urban area

(which are no longer used for exploitation and are now solely dedicated to MAR) (Wang et al., 2017).

The locations of all these exploiting wells, MAR wells, and MAR river segments are marked in Fig.6(b).

2.2. Groundwater sampling and recharge percentage quantification analysis

In the study area, surface water is the primary source of MAR. In order (To understand the current water quality status of karst groundwater and surface water in the study area, identifying the hydrochemical components in surface water that may influence groundwater quality, estimate the percentage contribution of surface water and precipitation recharge to karst groundwater, and to provide a basis for the groundwater flow and solute transport model setup, sampling and analysis of groundwater and surface water in the study area were conducted in June 2022. The analyzed indicators included total dissolved solids (TDS), sulphate concentration, nitrate concentration, chloride concentration, δ²H‰, and δ¹80‰. The locations of the sampling points are shown in Fig. 5(b).

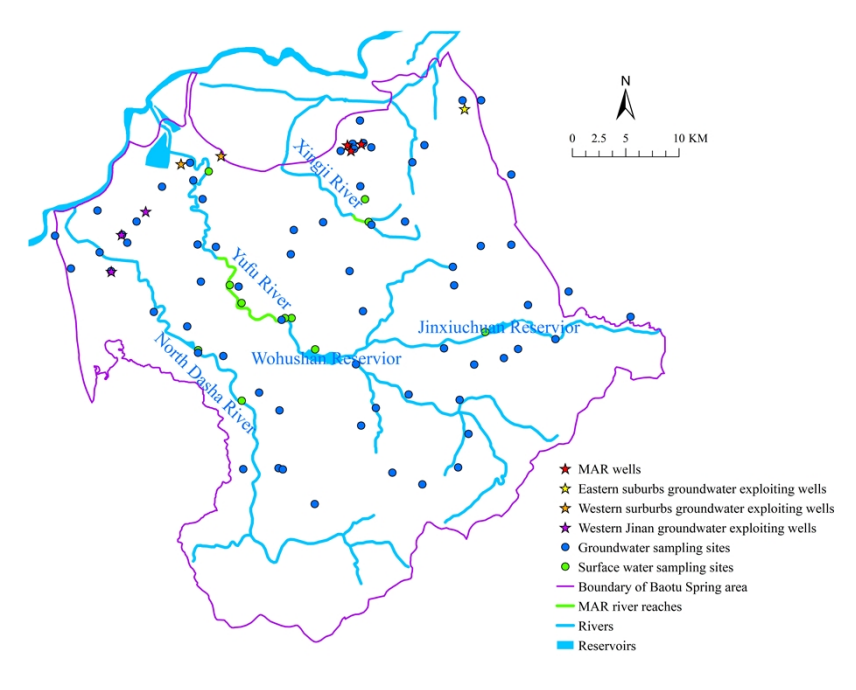


Fig.2 Locations of wells and sampling sites

After the analysis of groundwater and surface water samples, the origin and recharge sources of karst groundwater were determined by utilizing the $\delta^2 H\%$ and $\delta^{18}O\%$ scatter plot of groundwater and surface water. The analysis of 2H and ^{18}O requires referencing the Global Meteoric Water Line (GMWL) and the Local Meteoric Water Line (LMWL). The GMWL is given as (Craig, 1961):

$$\delta^2 H = 8\delta^{18} O + 10$$
 (1)

Using the China Meteoric Water Line (CMWL) as the LMWL for the study area, which is:

$$\delta^2 H = 7.7 \delta^{18} O + 7$$
 (2)

Then, to quantitatively analyze the impacteffect of MAR from surface water on karst groundwater, $\delta^2 H\%$ and $\delta^{18} O\%$ values were used to determine the proportion of groundwater recharge from surface water. Groundwater in the study area has two main recharge sources: surface water and precipitation (Liu et al., 2021). An improved two-end-member mixing model was employed to calculate the mixing ratios

of surface water and precipitation in groundwater samples. Assuming $\delta^2 H\%$ and $\delta^{18}O\%$ values for surface water are x_s and y_s , for precipitation are x_p and y_p , and for groundwater are x_g and y_g , the mixing ratios from surface water (η_s) and precipitation (η_p) were calculated. The traditional two-end-member mixing model uses either $\delta^2 H\%$ or $\delta^{18}O\%$ data to calculate these ratios with the Equation:

$$\begin{cases}
\eta_s = \frac{x_g - x_p}{x_s - x_p} \\
\eta_p = \frac{x_s - x_p}{x_s - x_p}
\end{cases}$$
(3)

317 Or:

$$\begin{cases}
\eta_s = \frac{y_g - y_p}{y_s - y_p} \\
\eta_p = \frac{y_s - y_g}{y_s - y_p}
\end{cases}$$
(4)

Due to the complexity of hydrogeological conditions (there may be unknown recharge sources affecting groundwater isotope values) and the limitations in endmembers selection (isotopic values of precipitation and surface water also vary across different regions), groundwater samples do not completely fall on the mixing line between two end-members in the $\delta^2 H\% - \delta^{19}O\%$ diagram. For certain samples located far from the mixing line (such as Point A in Fig. 2), calculating the mixing ratio using Eq. 3 or 4 essentially involves projecting sample Point A along the X- or Y-axis to Points $A_{(3)}$ or $A_{(4)}$ respectively, which may lead to significantly different results. To address this issue, this study proposes a method for computing the mixing ratio by projecting groundwater sample points onto the two-endmember mixing line in the $\delta^2 H\% - \delta^{18}O\%$ diagram (it is reasonable to assume that using the closest point on the mixing line, i.e., the orthogonal projection of the sample point $A_{(5)}$, yields a more reliable mixing ratio). For some samples, the mixing ratios calculated using Equation (3) or (4) differ significantly. This paper proposes a method that calculates the mixing ratio by projecting groundwater sample points onto the precipitation-surface water mixing line in a $\delta^2 H\% - \delta^{18}O\%$ diagram. The derived Equation for calculating the mixing ratio is as follows:

333
$$\eta_{S} = \frac{(x_{s} - x_{p})^{2} + (y_{s} - y_{p})^{2}}{(x_{s} - x_{p}) + (y_{s} - y_{p})(y_{s} - y_{p})}$$

$$\eta_{p} = \frac{(x_{s} - x_{p})^{2} + (y_{s} - y_{p})^{2}}{(x_{s} - x_{p})^{2} + (y_{s} - y_{p})^{2}}$$

$$A_{(3)}$$

$$A_{(4)}$$
A: Sample point
$$A_{(3)}$$
A: Sample point
$$A_{(3)}$$
Projection point of A onto the mixing line along the x-axis direction (Eq. 3)
$$A_{(6)}$$
Projection point of A onto the mixing line along the y-axis direction (Eq. 4)
$$A_{(6)}$$
Projection point of A onto the mixing line along the y-axis direction (Eq. 4)
$$A_{(6)}$$
Projection point of A onto the mixing line along the y-axis direction (Eq. 4)
$$A_{(6)}$$
Projection point of A onto the mixing line along the y-axis direction (Eq. 4)
$$A_{(6)}$$
Projection point of A onto the mixing line (Eq. 5)

-65

334 335

336

337

338

339

340

341

342

343

344

345

346

347

_9

Fig. 2 Schematic diagram illustrating the method for calculating two-endmember mixing proportions

 $\delta^{18}O\%$

-6

-8

In this research, the minimum $\delta^2H\%$ and $\delta^{18}O\%$ values of karst groundwater samples are considered as the values of precipitation recharge end-members, which are -64.56 and -9.30, respectively. The average $\delta^2H\%$ and $\delta^{18}O\%$ values of surface water samples are considered as the values of surface water recharge end-members, which are -50.53 and -6.815, respectively. Using Eq. 5, the mixing ratio for all karst groundwater samples could be calculated. It should be noted that although unauthorized sewage discharge might influence groundwater isotopic values, strict pollution controls in the study area (given Baotu Spring's significance) make this factor negligible for this study.

2.3. Infiltration test and flow monitoring of riversFlow monitoring and infiltration test

Based on field surveys, a large volume of released water in the Yufu River results in some flow escaping downstream and failing to infiltrate and recharge karst groundwater, thereby reducing the effective MAR rate. To verify this and investigate the infiltration capacity of an MAR river segments, elected five equidistant sites along the MAR segment of Yufu River and measured the permeability

eoefficient of the riverbed based on in-situ double-ring infiltration test (Li et al., 2019) (Fig.3). Then, the infiltration coefficient of the Yufu River MAR segment was calculated using the double-ring infiltration test results. The theoretical maximum recharge capacity was then determined based on the river's area. Additionally, the flow monitoring data from multiple segments of the Yufu River and Xingji River from 2014 to 2016 were collected (Fig. 13). According to the principle of water balance, the difference in flow between the cross-sections of the MAR river segment is considered as the effective MAR rate. For Yufu River, the water is released in Section #1, and the effective MAR rate equals the difference between the flow rate at section #1 and section #5 (Eq. 6). For Xingji River, the water is released in sSection #6, and the effective MAR rate equals the difference between the flow rate at section #6 and sSection #7 (Eq. 6). Then, based on the statistical data of the water release rate, the quantitative relationship between the water release rate and the effective MAR rate is analyzed. $\begin{cases} Q_{Eff(Yu)} \equiv Q_1 = Q_5 \\ Q_{Eff(Xing)} \equiv Q_6 = Q_7 \end{cases}$ In the equation, $Q_{Eff(Yu)}$ and $Q_{Eff(Xing)}$ denote the effective MAR rates of the Yufu River and the Xingji River, respectively, while Q_1 through Q_7 represent the flow rates of section #1 to section #7, correspondingly. It should be noted that although the 2014~2016 flow monitoring data from two hydrological years are sufficiently representative (reflecting the stable infiltration capacity of the river channels, as no largescale construction occurred after 2016), it remains necessary to calculate the maximum infiltration capacity to account for scenarios requiring high water release rates during extreme dry years or months. Therefore, we selected five sites along the MAR segment of Yufu River and measured the permeability coefficient of the riverbed based on in-situ double-ring infiltration test (Li et al., 2019) (Fig. 13). The infiltration test was performed at the riverbed edges (the river still maintains a small flow during the dry

348

349

350

351

352

353

354

355

356

357

358

359

360

361

362

363

364

365

366

367

368

season). Then, the infiltration coefficient of the Yufu River MAR segments was were calculated using the double-ring infiltration test results. The theoretical maximum recharge capacity was finally then determined based on the river's area.

Additionally,

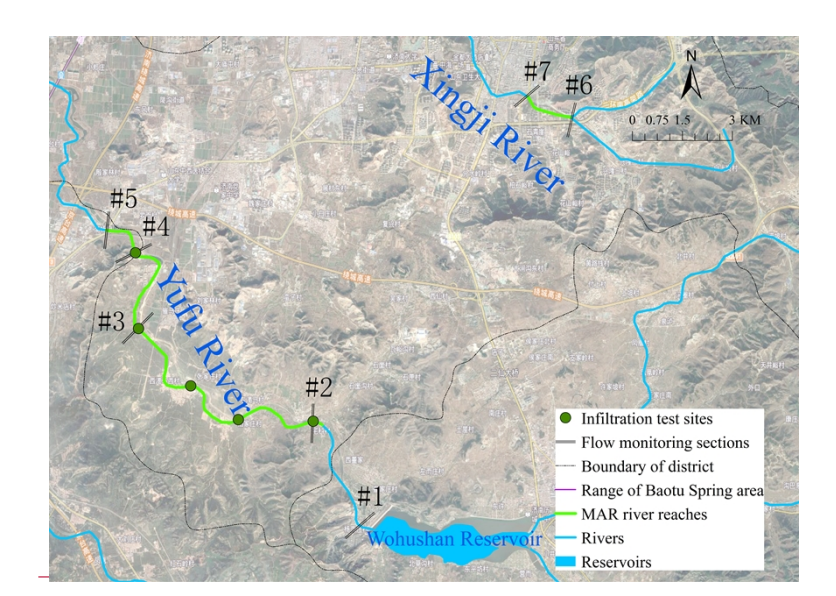


Fig.3 The locations and field photographs of infiltration test sites and flow monitoring sections

2.4. Estimation of effective porosity from tracer tests

Effective porosity is a crucial parameter for simulating groundwater solute transport. The actual groundwater velocity determined by tracer tests can be used to calculate the effective porosity of karst fissured aquifers (Zuber & Motyka, 1994), using the following Equation:

$$n_f = \frac{\kappa_I}{v_r} \tag{7}$$

This Equation is derived based on from Darcy's Llaw. In the equation, "K" represents the hydraulic conductivity (m/d), "I" is the hydraulic gradient, and " v_i " is the actual groundwater velocity (referring to the advective flow velocities governing the transport). There are tTwo large-scale tracer tests which have

been were conducted at Cuima village in year 1989 and in Xingji River in year 2016 (Zhu et al., 2020). To determine the parameters required in the groundwater solute transport model, the actual groundwater flow velocity and the effective porosity of the karst aquifer were calculated based on the data from the two tracer tests (Fig.,3).

First, three groundwater flow lines were extracted from the groundwater flow field, and several calculation points for groundwater flow velocity and effective porosity were selected at equal intervals. Flow lines #1 and #2 represent the diffusion direction of the tracers from Cuima Village, while flow line #3 represents the diffusion direction of the tracers from Xingji River. Using the isochrone map of tracer peak concentration diffusion, the actual groundwater flow velocity was calculated based on the horizontal distance between adjacent isochrones at each calculation point. The hydraulic gradient at the calculation points on flow lines #1 and #2 was calculated using 1989 groundwater level monitoring data, and the hydraulic gradient on flow line #3 was calculated using 2016 data. The permeability coefficient (K) for each calculation point was determined using the groundwater flow model established in this research.

Finally, the effective porosity at each calculation point was calculated using Eq. 7.

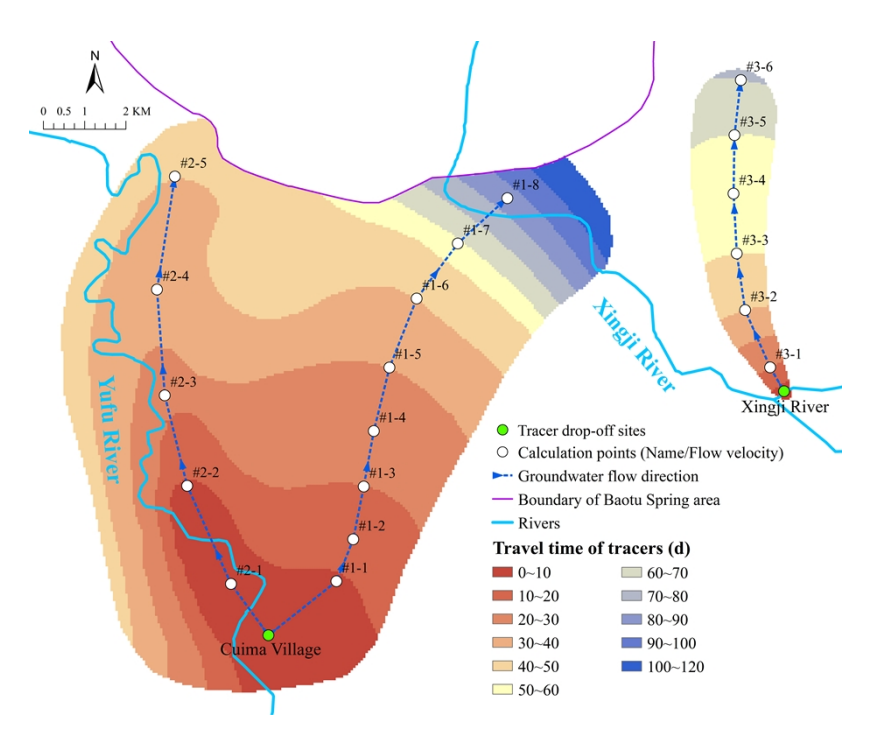


Fig. 3 Tracer tests conducted in Cuima Village and Xingji River

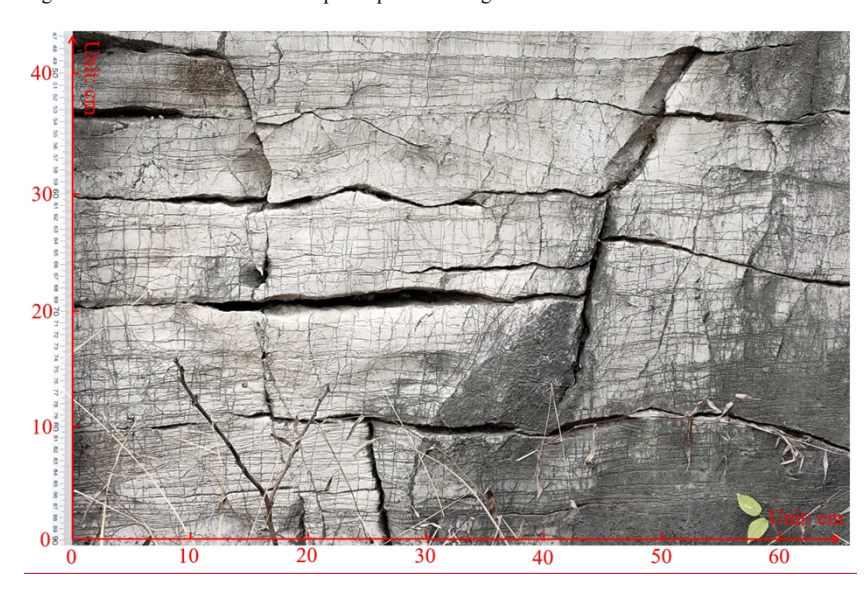
2.5. Groundwater flow-solute transport simulation

Numerical simulation is used to predict groundwater level and quality in this research. As mentioned in the introduction, the EPM model without inserting embedded karst-conduits embedded is capable for groundwater flow simulation in karst regions with low development like the northern China karst areas.

To verify this, we identified some typical karst fissure outcrops in the Ordovician limestone exposure area (Fig. 4) and measured the mechanical apertures of the fissures. The measurements show that the maximum mechanical aperture of the karst fissures is approximately 6 mm, while the minimum is less than 1 mm. For natural karst fissures, the hydraulic aperture used for flow calculations is typically much smaller than the mechanical aperture, with their ratio (generally less than 0.15 for karst fissures) determined by the fissure geometry and filling characteristics (Zhang & Nemcik, 2013; Zimmerman & Bodvarsson, 1996). For conservatism, we set the mechanical aperture at 6 mm and the ratio of hydraulic

aperture to mechanical aperture at 0.15 to determine the maximum Reynolds number (Re). Based on the findings in Section 3.3 (Tab.1 provided in the Supplement), the maximum actual groundwater flow velocity in the study area's runoff zone is approximately 216 m/d (0.0025 m/s). Using these data, Eq. 8 yields a rough estimate indicating that the Re of karst groundwater flow in the study area (\leq 2.24) is significantly lower than the critical Re (2000). Therefore, the flow regime in the karst fissures is laminar, justifying the use of the EPM model for simulation.

Consequently, the GMS software was used to establish a karst groundwater flow and solute transport model for the Baotu Spring area. The MODFLOW 2005 and MT3DMS packages were employed to solve the groundwater flow and solute transport equations using the finite difference method.



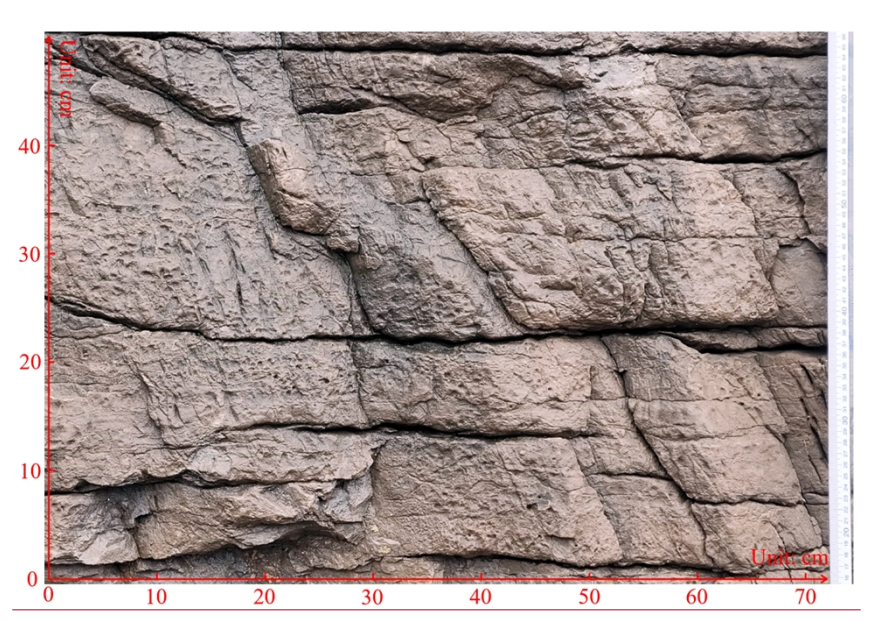


Fig. 4 Outcrop of karst fissures in the study area

424
$$\underline{Re} = \frac{\rho vL}{\mu} \le \frac{998 \times 0.0025 \times 0.006 \times 0.15}{1.002 \times 10^{-3}} = 2.24$$
 (8)

Where, Re: Reynolds number (dimensionless);

ρ: Fluid density (kg/m³);

v: Characteristic flow velocity (m/s);

L: Characteristic length (m), defined here as the hydraulic aperture of the fissures;

<u>μ</u>: Fluid dynamic viscosity (kg/(m.s)).

The numerical model encompasses the Baotu Spring area, simplifying the stratigraphy into four units: Quaternary porouspore phreatic aquifer, intrusive rock aquitard, Ordovician-Cambrian karst aquifer, and the aquitard below the Mantou Formation (Fig. 5(a)). The Ordovician-Cambrian karst aquifer is the main aquifer and the target aquifer for MAR and groundwater extraction exploitation. In Fig. 5(a), the vertical (Z-axis) scale is exaggerated fivefold to enhance the visualization of topographic undulations and stratigraphic profile variations. The boundaries of the Ordovician-Cambrian karst

aquifer are delineated inset as Fig. 5(b). Additionally, the boundaries of other strata are all impervious. The model's source and sink terms include precipitation recharge, MAR from rivers and wells, groundwater extractionexploitation, spring discharge, agricultural irrigation extractionexploitation, and agricultural irrigation re-infiltration. Precipitation recharge is calculated based on precipitation quantity, infiltration recharge coefficient, and recharge zone area. The infiltration recharge coefficient accounts foreonsiders surface lithology, urbanization, and agricultural development. The MAR from rivers mainly occur through the Yufu and Xingji Rivers, and the aetual MAR rateeffective MAR rate is discussed in Section 3.2. The locations of MAR wells, groundwater exploiting extracting wells and MAR river segments are displayed in Fig. 5(b). The hydraulic conductivity K consists of horizontal hydraulic conductivity K_x and vertical hydraulic conductivity K_y . The zoning and values of K_x are mainly based on the hydrogeological tests, and then identified and verified using groundwater level monitoring well data. K_y is uniformly set to 0.1 times K_x . The remaining hydrogeological parameters (specific yield, storativitystorage coefficient, and dispersivity dispersity) are taken as empirical values. The determination of effective porosity has been discussed in Section 2.4. The simulation period spans from January 1, 2020, to December 31, 2022, with each stress period lasting one month. Next, the impacteffect of MAR and groundwater exploitation extraction on the dynamics of karst groundwater levels was quantitatively analyzed using a groundwater flow model, with Baotu Spring's water level serving as a representative indicator. The considered MAR are from Yufu River, Xingji River, and MAR wells. For the simulation period of 2020-2022, the net variations of Baotu Spring water level caused by MAR and groundwater extraction exploitation were calculated.

436

437

438

439

440

441

442

443

444

445

446

447

448

449

450

451

452

453

454

455

456

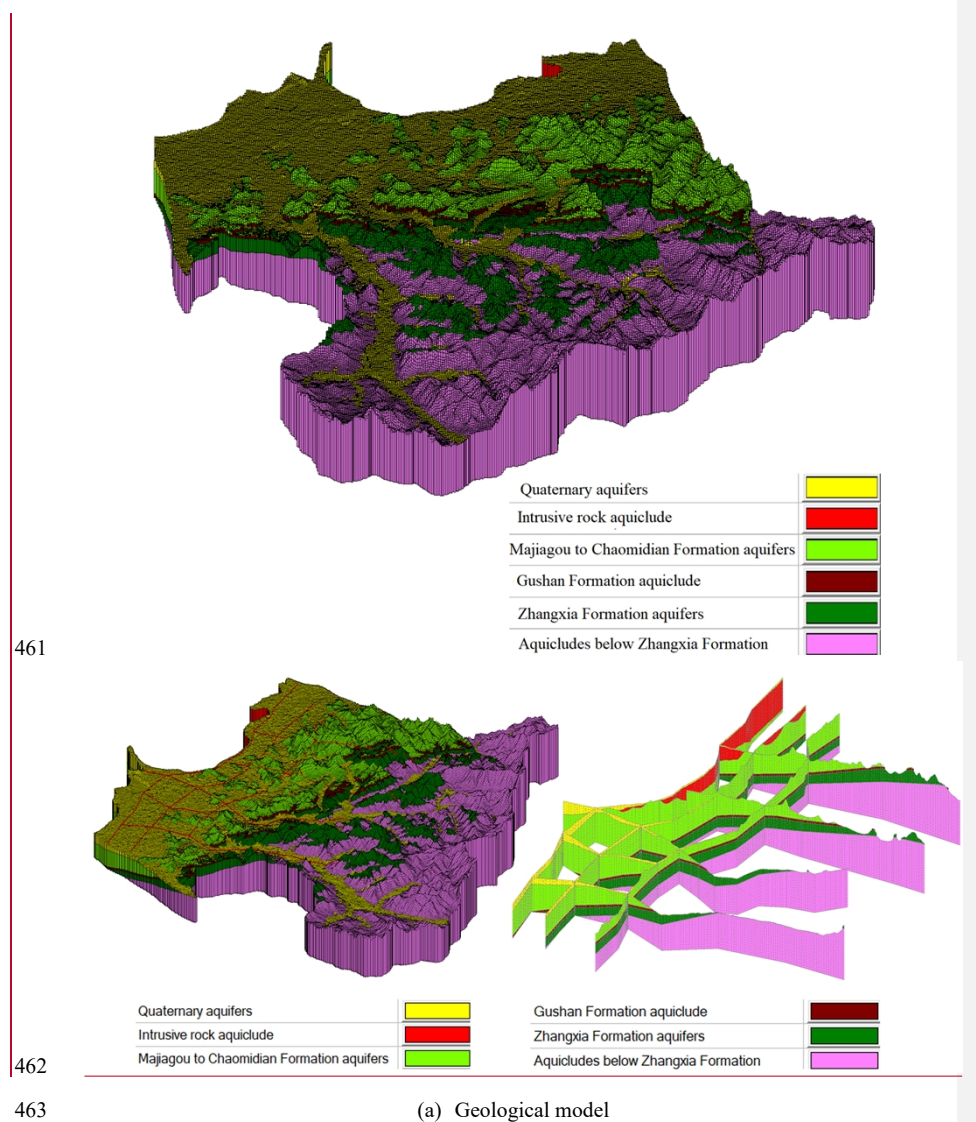
457

Finally, to quantitatively compare the effects of various MAR and groundwater

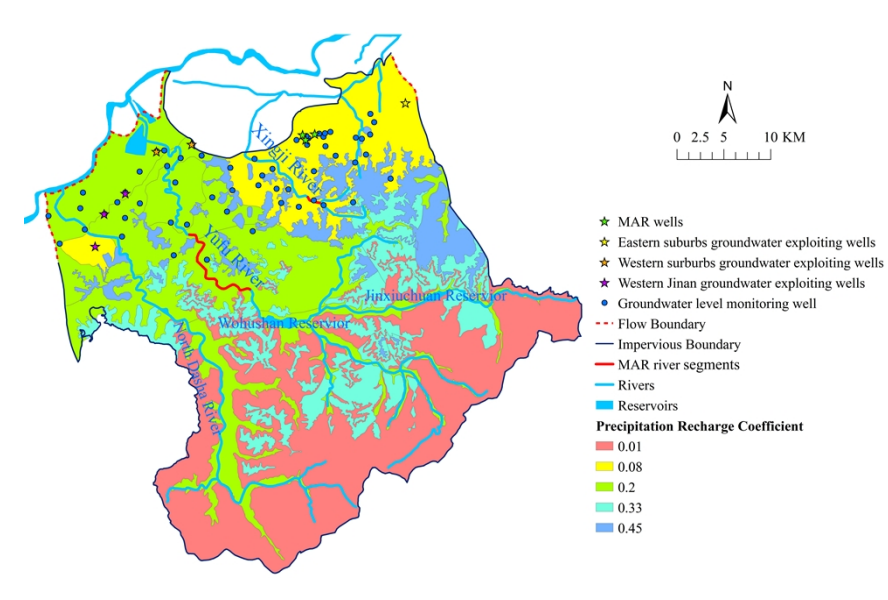
458 $\underline{\text{extraction}} \underline{\text{exploitation}} \text{ on the dynamics of Baotu Spring water level, the water level net variation after 1,}$

2, and 3 years of continuous recharge and extraction exploitation at a constant flow rate was calculated

460 and compared.



(a) Geological model



465 (b) Settings of groundwater flow model

Fig. 5 Geological model and groundwater flow model

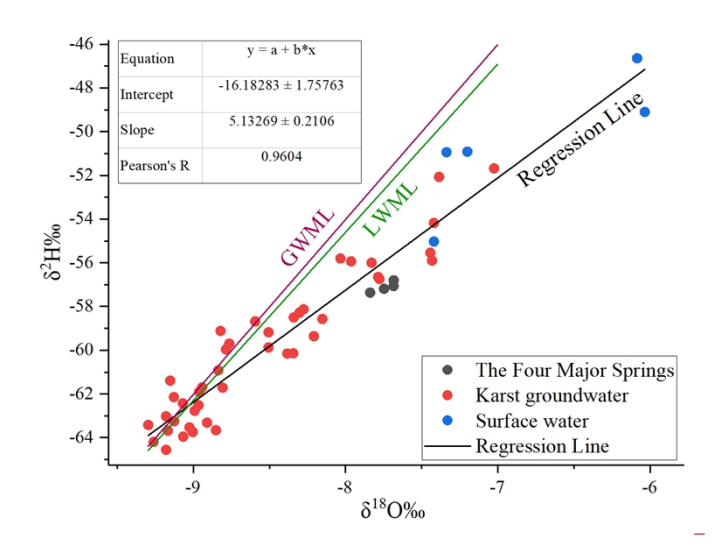
For the solute transport simulation, sulphate is selected as the representative solute because its concentration in the surface water used for MAR is higher than that-in the groundwater, while the concentrations of other solute components are either similar to or lower than those in the groundwater. The simulation is based on the groundwater flow model from-spanning 2020 to 2022, with all recharge/discharge values averaged over this period to mitigate seasonal flow variations. The initial sulphate concentration in karst groundwater is uniformly set at 50 mg/L, reflecting the average concentration in high-quality water from the wells in western suburbs. The model then simulates the dynamics of sulphate concentration in karst groundwater after 2, 6, and 18 months of continuous recharge with sulphate concentrations of 150 mg/L, 250 mg/L, and 350 mg/L in the MAR water.

3. Results and Discussion

3.1. Mixing percentages of groundwater recharge sources

A scatter plot of the $\delta^2 H\%$ and $\delta^{18} O\%$ of groundwater and surface water is generated in Fig. 6. It

shows that karst groundwater samples are distributed near the LMWL, indicating that the karst groundwater in the study area originates from precipitation (Liu et al., 2021). The isotopic enrichment of ²H and ¹⁸O in surface water samples is significantly higher than that in karst groundwater samples, exhibiting a typical evaporation effect. Additionally, the karst groundwater samples gradually deviate from the LMWL with the enrichment of ²H and ¹⁸O, indicating the mixing of precipitation and surface water. This suggests that the karst groundwater is significantly recharged by surface water.



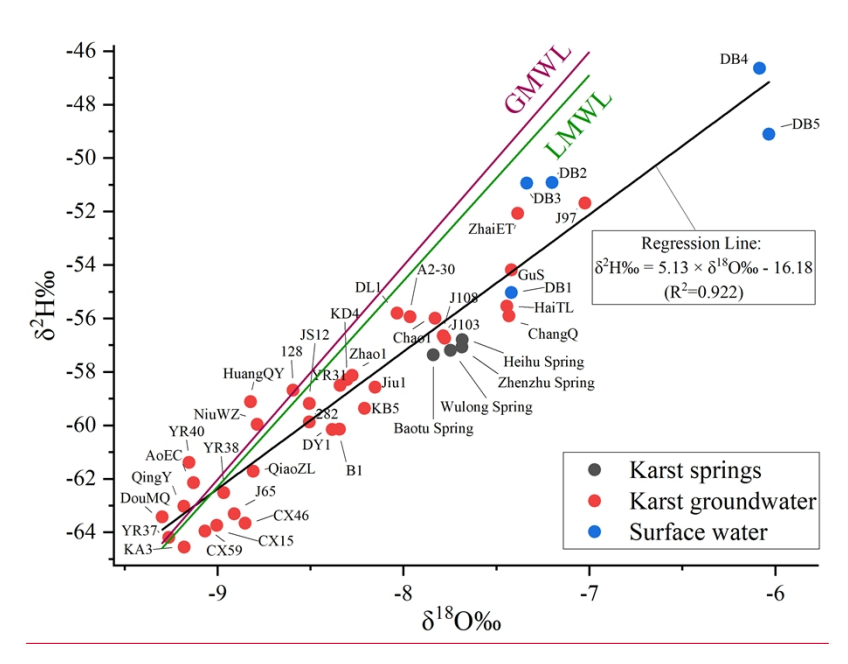
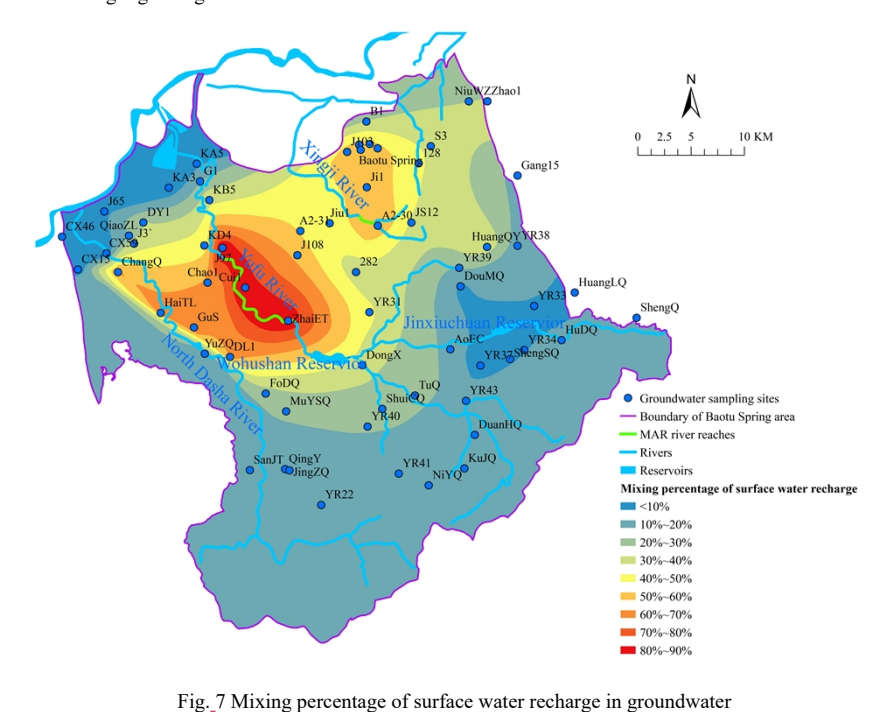


Fig._6 Scatter plot of $\delta^2 H\%$ and $\delta^{18} O\%$ in water samples

Previous studies have quantitatively calculated the contribution rates of groundwater flow from different strata to the four major springs in the Baotu Spring area of Jinan City, demonstrating varying groundwater circulation depths among these springs (Zhu et al., 2020). However, despite originating from different stratigraphic layers, the ultimate source of groundwater flow remains precipitation and surface water (Guo et al., 2019). To better evaluate MAR effects primarily conducted through river channels, it is essential to determine the proportion and spatiotemporal distribution characteristics of surface water recharge in groundwater—an aspect not addressed in prior research.

In this study, Tthe mixing percentage of surface water recharge in groundwater is calculated with Eq. 5 and exhibited in Fig. 7. According to the result, the closer the distance to the MAR segments of Yufu River and Xingji River is, the higher the mixing percentage of surface water recharge in groundwater. In the southern metamorphic rock and Cambrian Zhangxia Formation limestone outcrop

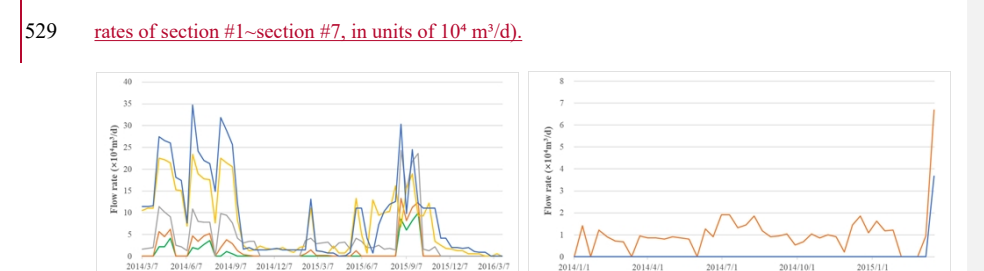
areas, as well as the northwestern Yellow River alluvial plain, the mixing percentage of surface water recharge is generally less than 20%. In contrast, in the middle and lower segments of the Yufu River and North Dasha River basins, as well as the Xingji River basin, the mixing percentage of surface water recharge is relatively high. The highest mixing percentage is near the MAR segments of the Yufu River and Xingji River. For example, in the villages along the MAR segment of the Yufu River, the mixing percentage of surface water recharge in wells ZhaiET, Cui1, and J97 exceeds 80%, while in wells A2-30 and Ji1 near the Xingji River MAR segment, and the Springs downstream, it exceeds 50%. These results highlight that the MAR from the Yufu River and Xingji River is a significant component of karst groundwater resources, emphasizing the importance of MAR projects in ensuring groundwater resources and raising regional groundwater levels.



3.2. Infiltration efficiency of MAR river segments

According to the test results of in-situ double-ring infiltration test, the bed permeability coefficient of the Yufu River MAR segment ranges from 1.96 to 2.76 m/d, with an average of 2.30 m/d across five sites. According to high-resolution satellite images, the Yufu River MAR segments (Fig.4), from Section #1 to Section #5, approximately covers an area of 0.50 km². Assuming a vertical infiltration hydraulic gradient of 1, the theoretical maximum MAR rate for the Yufu River MAR segments, calculated using Darcy's Law, is approximately 114.9×104m²/d.

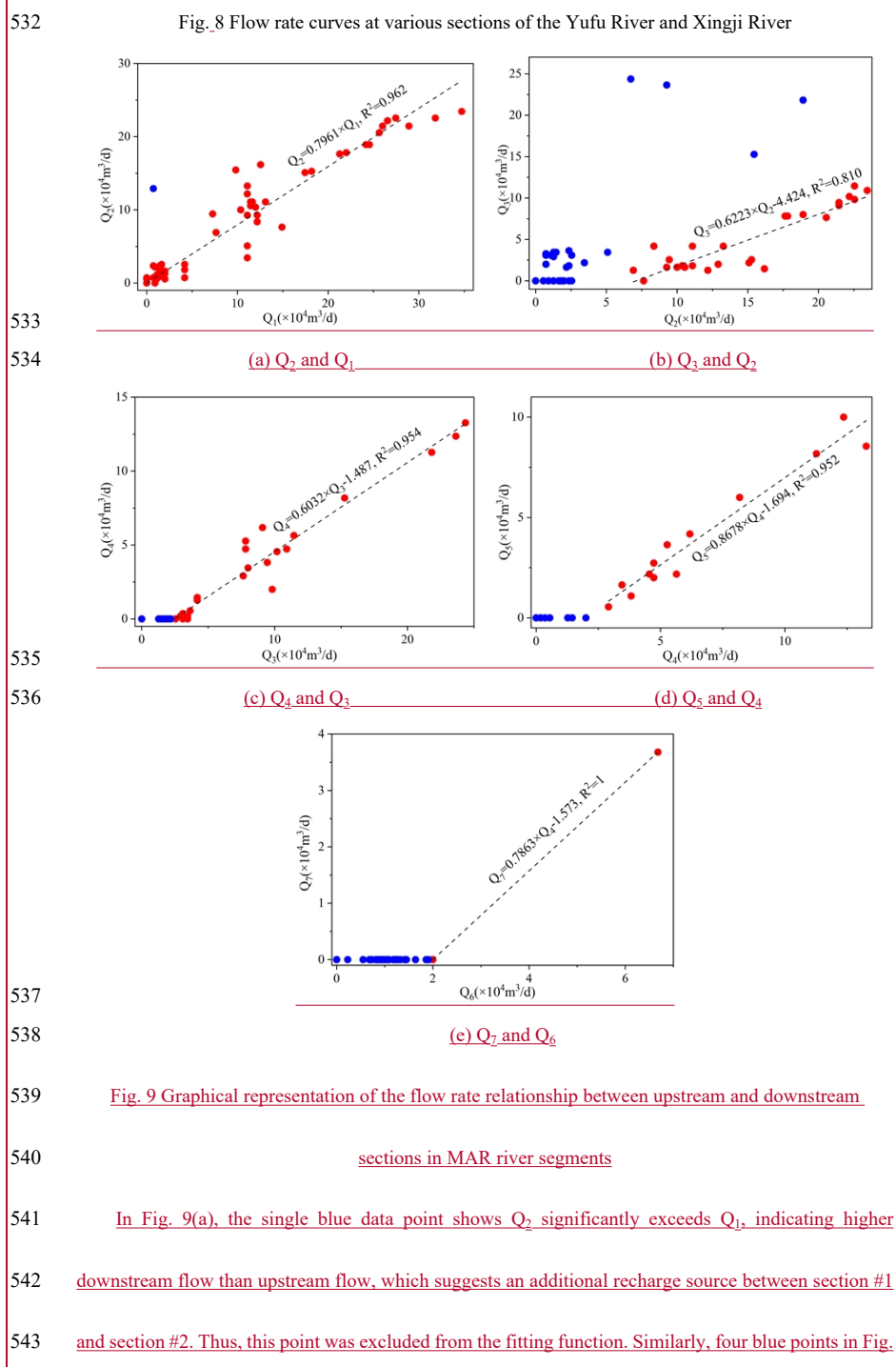
Based on field surveys, large volume of released water in the Yufu River results in some flow escaping at the Section #5, failing to infiltrate and recharge karst-groundwater, thereby reducing the actual MAR rate. To verify this, Firstly, in order to investigate the relationship between effective MAR rates and water release rates, we analyzed flow data from 2014 to 2016 (Fig. 8), analysis of flow data from 2014 to 2016 (Fig. 8) was conducted, revealing the relationship between actual MAR rates and water release-rates. Since the MAR segment of the Yufu River is divided into four segments by five flow monitoring sections, whereas Xingji River has only one MAR segment due to a single upstream and downstream section, the upstream and downstream flow rates were analyzed separately for each segment



to assess groundwater infiltration capacity. Based on the data in Fig. 8, we plotted the flow relationships

between upstream and downstream sections for each segment (Fig. 9, where Q1~Q7 represent the flow

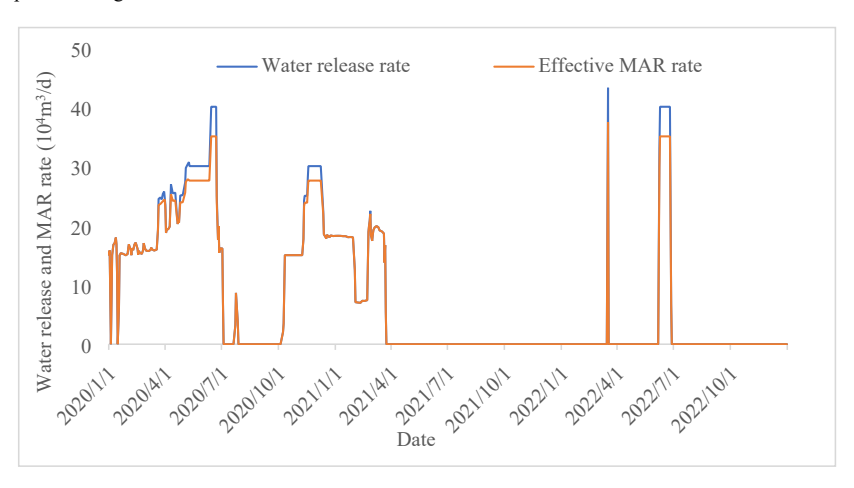
531 (a) Yufu River (b) Xingji River

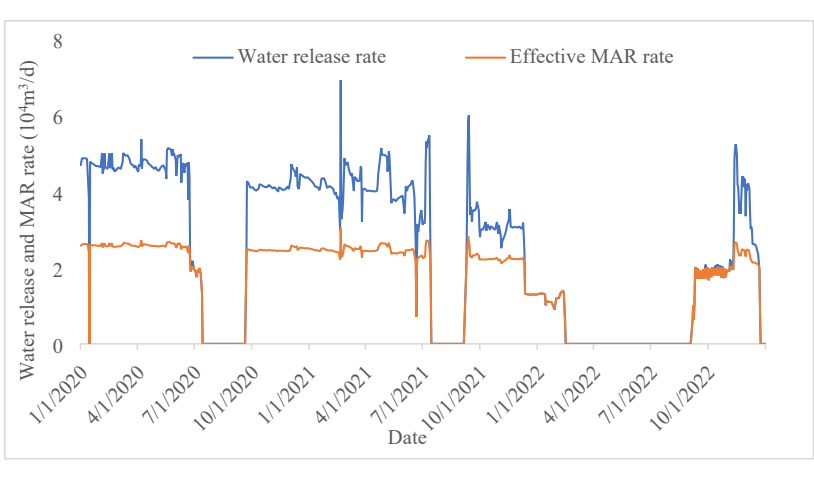


9(b) that deviate markedly from the fitted line were also excluded. Furthermore, Figures 9(b)-9(e) show 545 that when upstream flow is low, downstream flow is nearly zero, suggesting complete infiltration of river 546 water into groundwater below a certain threshold of flow, defined as the "critical flow rate." Data analysis 547 reveals that when flow exceeds this critical flow rate (Eq. 9), upstream and downstream flows generally 548 follow a linear relationship (Eq. 9), with Pearson R² all exceeding 0.810. (1). $Q_2 = 0.7961 \times Q_1 \cdot (Q_1 \ge 0, R^2 = 0.962)$ (2). $Q_3 = 0.6223 \times Q_2 = 4.424 (Q_2 > 7.109, R^2 = 0.810)$ (3). $Q_4 = 0.6032 \times Q_3 = 1.487 (Q_3 > 2.465, R^2 = 0.954)$ (4). $Q_5 = 0.8678 \times Q_4 = 1.694 (Q_4 > 1.952, R^2 = 0.952)$ 549 (9) (5). $Q_7 = 0.7863 \times Q_6 = 1.572 (Q_6 \ge 2.R^2 = 1)$ 550 Then, by combining Eq. 9 with Eq.6, the following relationships are established: the effective MAR 551 rate in the Yufu River is quantitatively related to Q_I (Eq. 10), while that of the Xingji River correlates 552 with Q_6 (Eq. 11). $\begin{cases} Q_{Eff(Yu)} \equiv Q_{1} \quad (Q_{1} \le 20.44) \\ Q_{Eff(Yu)} \equiv 0.7449Q_{1} + 5.214 \quad (Q_{1} \ge 20.44) - 0.00 \end{cases}$ 553 (10) $\begin{cases} Q_{Eff(Xing)} \equiv Q_6 \ (Q_6 \le 2) \\ Q_{Eff(Xing)} \equiv 0.2137 Q_6 \pm 1.573 \ (Q_6 \ge 2) - 10 \end{cases}$ 554 (11) 555 In the equation, the units of Q_1 to Q_7 , as well as $Q_{Eff(Yu)}$ and $Q_{Eff(Xing)}$, are all 10^4 m³/d. 556 According to Eq. 10, when the water release rate does not exceed 20.44×10⁴m³/d, the effective MAR 557 rate for Yufu River equals the water release rate, indicating full infiltration of surface water before section 558 #5. However, when the water release rate exceeds 20.44×10⁴m³/d, the effective MAR rate is less than 559 the water release rate, as some surface water flows past section #5 without complete infiltration. Similarly, 560 Eq. 11 demonstrates that the Xingji River follows a similar pattern to the Yufu River. 561 When the water release rate does not exceed 21.6×10⁴m³/d, the actual MAR rate equals the water 562 release rate, indicating full infiltration of surface water before Section #5. However, when the water 563 release rate exceeds 21.6×10⁴m³/d, the actual MAR rate is less than the water release rate, as some surface 564 water flows past Section #5 without infiltrating karst groundwater. Calculations confirm that when the

565 water release rate exceeds 21.6×104m³/d, the relationship between the actual MAR rate and the water 566 release rate follows Equation (7). 567 $Q_{Aet} = 0.843 \times Q_{Rel} + 3.396$ 568 Where, QAet is the actual MAR rate in Yufu River (m²/d), and QRel is the water release rate in Yufu 569 River Section #1 (m³/d). 570 Likewise, in Xingji River, the relationship between the actual MAR rate and the water release rate 571 follows Equation (8) when the water release rate exceeds 2×10⁴m³/d. 572 $Q_{Aet} = 0.214 \times Q_{Rel} + 1.573$ 573 Where, Q_{Aet} is the actual MAR rate in Xingji River (m³/d), and Q_{Rel} is the water release rate in Xingji 574 River Section #6 (m³/d). 575 According to the test results of in -situ double-ring infiltration test, the streambed permeability 576 coefficient of the Yufu River MAR segment ranges from 1.96 to 2.76 m/d, with an average of 2.30 m/d 577 across five sites. According to high-resolution satellite images, the Yufu River MAR segments (Fig. 14), 578 from sSection #1 to sSection #5, approximately covers an area of 0.50 km². Assuming a vertical 579 infiltration hydraulic gradient of 1, the theoretical maximum MAR rate for the Yufu River MAR 580 segments, calculated using Darcy's Law, is approximately 114.9×10⁴m³/d. It should be noted that during 581 the monitoring period (2014-2016), the maximum flow rate of the Yufu River was 34.73×10⁴ m³/d, much 582 $\underline{less \ than \ this \ value. \ This \ indicates \ that \ although \ a \ water \ release \ rate \ exceeding \ 20.44 \times 10^4 \ m^3/d \ may \ lead}}$ 583 to partial waste of recharge water, further increasing the water release rate can still enhance groundwater 584 recharge. 585 Finally, the effective MAR rates of the Yufu River and Xingji River from 2020 to 2022 werewas 586 calculated, as shown in Fig. 10, respectively. These calculations were used as surface water recharge

inputs for the groundwater flow model.





(a) Yufu River

(b) Xingji River

 $Fig._10\ Water\ release\ rate\ VS.\ Effective\ MAR\ rate\ in\ Yufu\ River\ and\ Xingji\ River$

3.3. Effective porosity of karst aquifers estimated from tracer tests

As discussed in Section 2.4, the effective porosity at each calculation point was calculated using Eq. 7, with the process and results shown in Tab.1 (provided in the Supplement). According to Tab.1, the groundwater flow velocity in the study area ranges from 52.4 to 216 m/d, Obviously, and the effective

porosity of the aquifer varies widely, with the maximum, minimum, and average values being 4.39×10⁻⁴, 1.28 × 10⁻⁵, and 1.08 × 10⁻⁴, respectively. Consistent with these findings, the effective porosity of Cretaceous Chalk in northeastern England's Yorkshire ranges from 3.7×10⁻⁴ to 4.1×10⁻³ (Agbotui et al., 2020), while Jurassic Limestone and Magnesian Limestone exhibit values of 1×10⁻⁴ (Foley et al., 2012) and 3×10⁻⁴ (Medici et al., 2019), respectively. This variability is closely related to the heterogeneity of the karst aquifer, aligning with studies in similar carbonate rock regions in the UK and Austria (Medici & West, 2021; Worthington et al., 2019). Studies have indicated that the effective porosity of karst systems exhibits significant scale effects, primarily attributed to the heterogeneity of groundwater flow velocities caused by the non-uniform development of karst conduits and fissures. For regional groundwater studies, large-scale tracer tests and dilution tests should be employed to determine the effective porosity, which typically ranges between 10⁻⁴ and 10⁻³—considerably lower than previously recommended values (0.1–0.01) (Medici & West, 2021). In this paper, the average effective porosity (1.08×10⁻⁴) from all calculated points on three flow lines from the Cuima Village and Xingji River tracer tests was used to represent the karst aquifer's effective porosity for groundwater solute transport modeling.

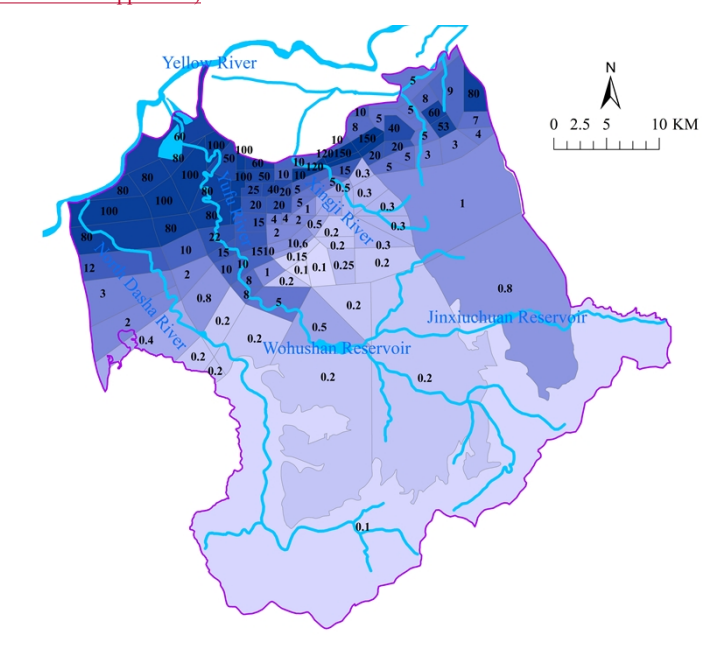
Tab.1 Effective porosity at the calculation points

Name	Flow velocity (m/d)	Permeability (m/d)	Hydraulic gradient	Effective porosity
#1-1	233.6	10	4.23E-03	1.81E-04
#1-2	240.3	4	3.85E-03	1.60E-05
#1-3	266.9	2	1.70E-03	1.28E-05
#1-4	295.2	4	1.16E-03	1.58E-05
#1-5	225.5	20	1.20E-03	1.07E-04
#1-6	148.3	20	3.85E-04	5.19E-05
#1-7	82.4	120	3.01E-04	4.39E-04
#1-8	52.4	10	3.07E-04	5.85E-05
#2-1	449.6	10	2.46E-03	5.47E-05
#2-2	293.2	22	1.03E-03	7.70E-05
#2-3	193.5	80	1.67E-04	6.89E-05
#2-4	356.3	80	2.78E-04	6.24E-05
#2-5	307	50	4.42E-04	7.21E-05

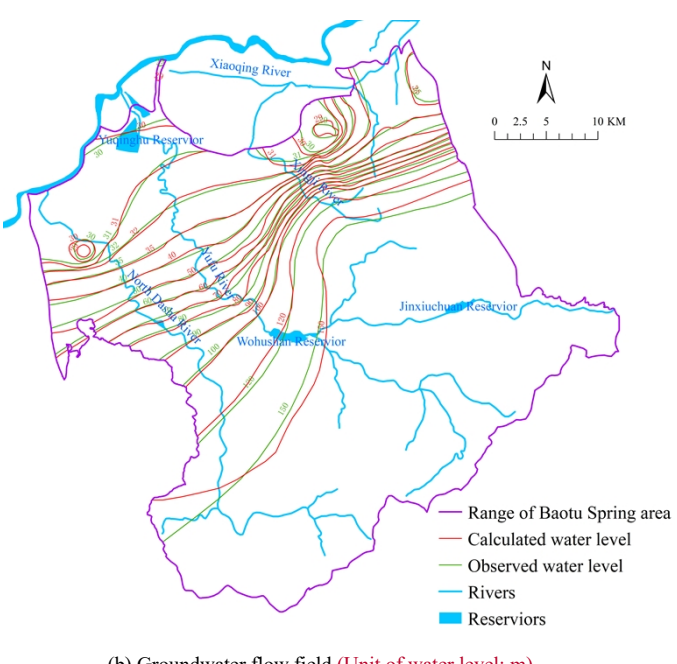
#3-1	63	0.3	1.07E-02	5.09E-05
#3-2	96.8	0.3	1.26E-02	3.90E-05
#3-3	165.1	4	1.29E-02	7.83E-05
		_		
#3-4	287.7	20	2.08E-03	1.45E-04
#3-5	275.7	120	9.88E-04	4.30E-04
#3-6	71.8	8	8.65E-04	9.64E-05
Max	449.6	<i>‡</i>	<i>‡</i>	4.39E-04
Min	52.4	<i>‡</i>	<i>‡</i>	1.28E-05
Average	216	4	<i>‡</i>	1.08E-04

$3.4. \, \underline{\textbf{Impact}}\underline{\textbf{Effect}} \, \textbf{s of MAR and } \underline{\textbf{groundwater}} \, \underline{\textbf{extraction}} \underline{\textbf{exploitation}} \, \textbf{on groundwater level}$

 According to the identification and verification of the groundwater flow model, the horizontal hydraulic conductivity of karst aquifers is exhibited-shown in Fig._11(a). The calculated and observed groundwater flow field as of December 31, 2022, are exhibited-shown in Fig._11(b), and the calculated and observed groundwater levels for the-representative monitoring wells are shown in Fig._11(c) to 11(f) (provided in the Supplement).



(a) Horizontal hydraulic conductivity of karst aquifers (Unit: m/d)

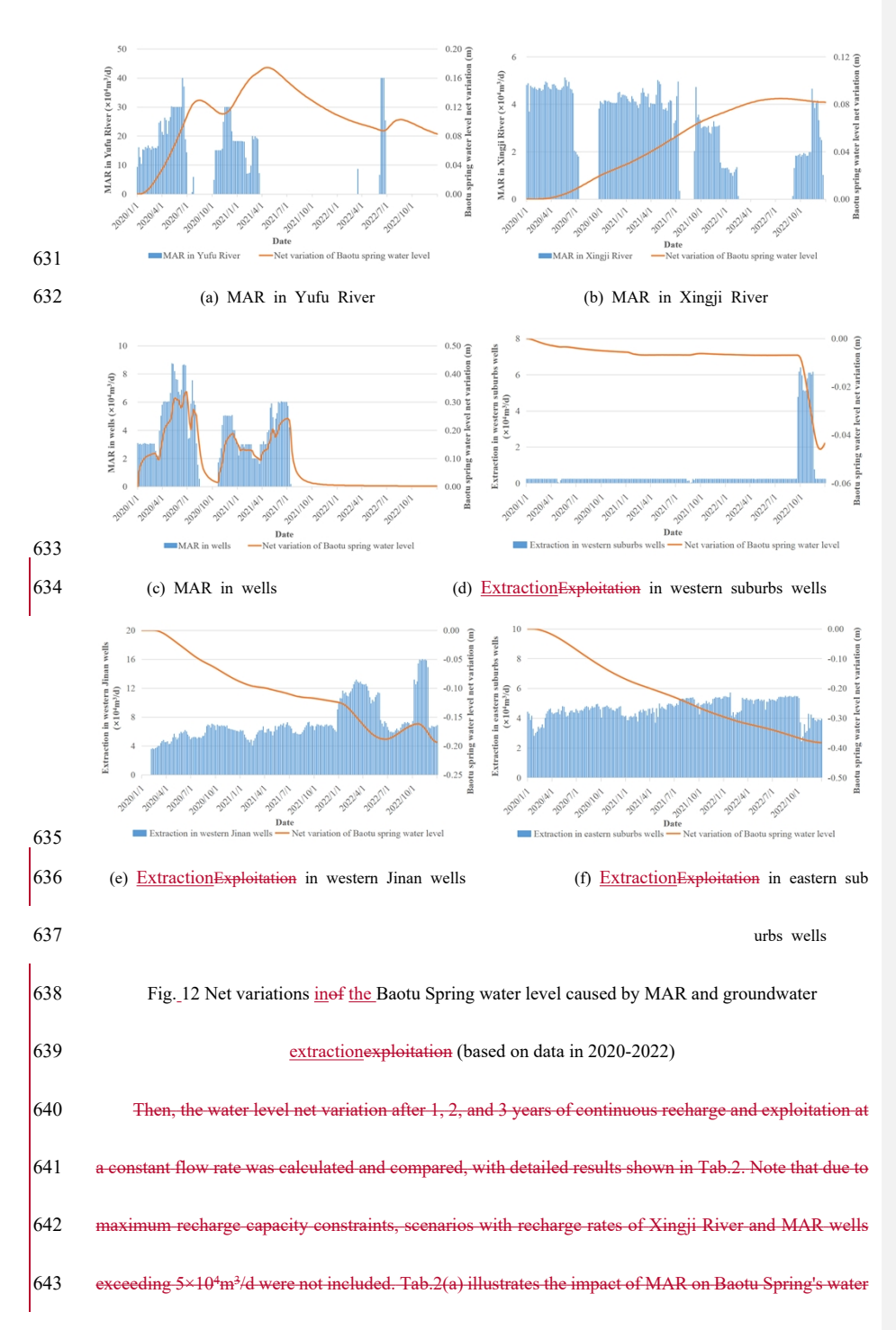


(b) Groundwater flow field (Unit of water level: m)

Fig._11 Identification and verification result of the groundwater flow model

The net variations of Baotu Spring water level caused by MAR and groundwater extractionexploitation were simulated and are displayed in Fig._12. The "net variations inof the Baotu Spring water level" in Fig._12 refers to the portion of groundwater level fluctuation in Baotu Spring caused by MAR and groundwater extractionexploitation. These variations are calculated using a numerical model based on actual MAR and groundwater extractionexploitation data. It shows that the water level of Baotu Spring rises with MAR and drops with groundwater extractionthe water level of Baotu Spring clearly rises with MAR and drops with groundwater exploitation. There is also a lag in the impacteffect of these factors on the water level.

Commented [HC1]: This figure has been modified. Panels c, d, e, f has been moved to Supplement Material.



level. It shows that, with the same recharge rate and duration, the MAR in wells has the greatest effect, followed by Xingji River, and Yufu River has the least impact. Despite this, Yufu River's maximum recharge capacity greatly exceeds that of Xingji River and the MAR wells. Additionally, the water level rise under MAR wells recharge remains almost unchanged within the three years, indicating that the maximum effect is achieved within the first year. This rapid response is due to the proximity of the MAR wells to Baotu Spring (0.75 km, 0.81 km, and 0.35 km, respectively) and the high permeability (k=150 m/d) of the shared karst aquifer. In practice, the most suitable MAR source should be chosen based on the following strategies. Firstly, MAR in wells yields the best results and raises the Baotu Spring water level the fastest, but it has a low maximum recharge capacity. Therefore, MAR in wells should be prioritized for a rapid short-term rise in the Baotu Spring water level. Secondly, MAR in Xingji River is less effective and also has a low maximum capacity, making it suitable for maintaining a small long-term rise in the Baotu Spring water level in conjunction with MAR in wells. Thirdly, MAR in Yufu River is the least effective but has a high maximum capacity, so for a significant long term rise in the Baotu Spring water level, all three sources should be considered, with MAR in Yufu River being the primary source. The water level net variation following continuous recharge and extraction at a constant flow rate over 1, 2, and 3 years was computed and compared, with results presented in Tab.2. Due to maximum recharge capacity limitations, scenarios exceeding 5×104 m³/d for Xingji River and MAR wells were excluded. Tab.2(a) demonstrates the impact of MAR on Baotu Spring's water level, revealing that wellbased MAR yields the greatest effect, followed by Xingji River, while Yufu River exhibits the least influence despite its substantially higher maximum recharge capacity. Notably, well-based MAR induces

644

645

646

647

648

649

650

651

652

653

654

655

656

657

658

659

660

661

662

663

664

665

minimal water level variation beyond the first year, attributable to their proximity to Baotu Spring (0.75

Tab. 2 The effect on groundwater level net variation at Baotu Spring resulting from a constant rate of

(a). The effect on groundwater level rise resulting from MAR

MAR rate (×10 ⁴ m ³ /d)		Duration of groundwater recharge		
		1 year	2 years	3 years
	2	19 mm	31 mm	36 mm
	5	49 mm	76 mm	90 mm
Yufu River	10	97 mm	152 mm	179 mm
	20	194 mm	300 mm	353 mm
	30	266 mm	409 mm	480 mm
	2	23 mm	60 mm	89 mm
Xingji River	5	38 mm	100 mm	148 mm
MAD. II	2	85 mm	86 mm	86 mm
MAR wells	5	212 mm	214 mm	216 mm

(b). The effect on groundwater level drop resulting from groundwater extraction exploitation

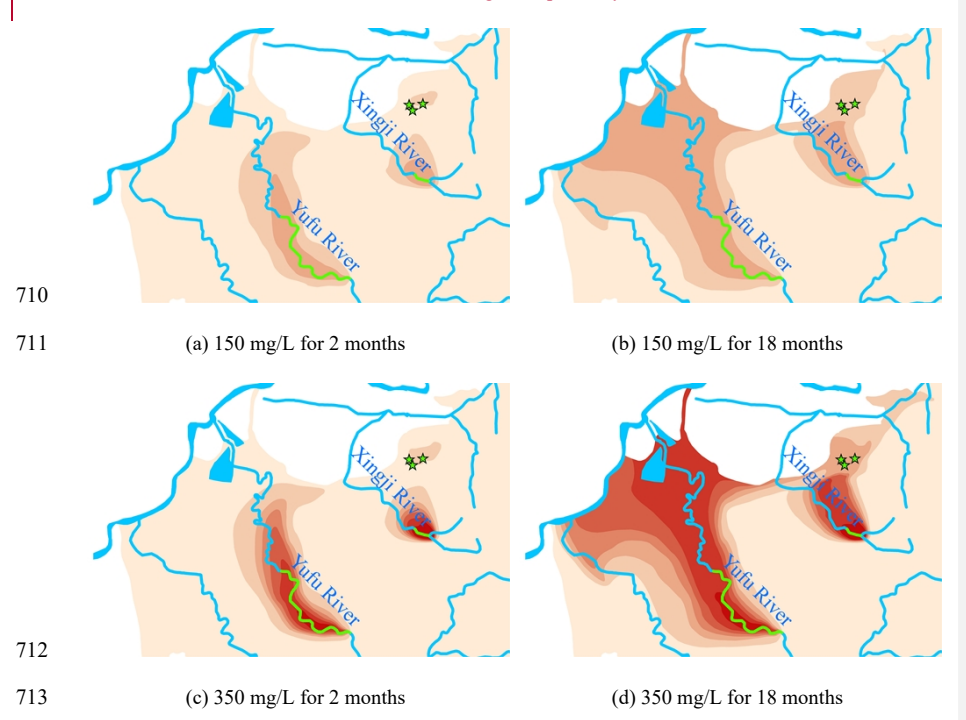
Groundwater extractioner	eploitation	Duration of groundwater extractionexploitation		
rate (×104m3/d)		1 year	2 years	3 years
Western suburbs wells	5	115 mm	138 mm	142 mm
western suburbs wells	10	230 mm	283 mm	293 mm
W . F 11	5	87 mm	106 mm	107 mm
Western Jinan wells	10	175 mm	218 mm	221 mm
	5	199 mm	322 mm	382 mm
Eastern suburbs wells	10	397 mm	643 mm	765 mm

3.5. ImpactEffects of MAR on groundwater quality

Based on the groundwater solute transport model established in this paper, simulations were conducted to monitor the dynamics of sulphate concentration in karst groundwater after continuous recharge of water with sulphate concentrations of 150 mg/L, 250 mg/L, and 350 mg/L over periods of 2 months, 6 months, and 18 months. As shown in Fig. 13 (The other subfigures of Fig. 13 are provided in the Supplement), with prolonged recharge duration and deteriorating recharge water quality, the sulphate concentrations in karst groundwater increase and the affected area of karst groundwater quality expands continuously, indicating an increasing impacteffect of MAR on karst groundwater quality over time. Therefore, deteriorating water quality from MAR poses risks to groundwater, and strict control and

monitoring of recharge water quality are necessary.

Additionally, sulphate concentrations in karst groundwater reach stability after 12—18 months of continuous recharge, and a linear regression established a quantitative relationship between the sulphate concentrations in karst groundwater and in MAR water (Fig._14). In practice, target values for sulphate concentrations in karst groundwater should be preset, and the minimum control standards for sulphate concentrations in MAR water could be calculated using the relationship shown in Fig._14. For example, according to China's Groundwater Quality Standards, the sulfate concentrations in Class I, II, and III groundwater must not exceed 50, 150 and 250 mg/L, respectively. Thus, it can be calculated that to ensure karst groundwater meets Class I, II, and III standards, the sulfate concentration in the MAR water source must not exceed 56.5, 197.8 and 339.1 mg/L, respectively.



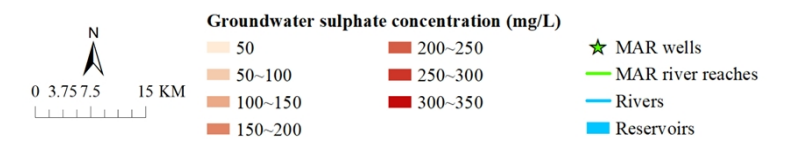


Fig. 13 Evolution of sulphate concentration in karst groundwater under MAR

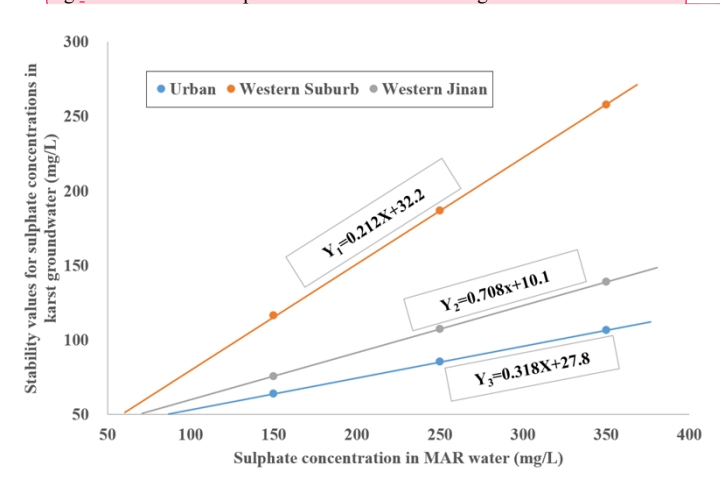


Fig.14 Linear relationships between sulphate concentrations in karst groundwater and MAR water

4. Conclusions

In this research, the impacts of MAR and groundwater exploitation on the dynamics of karst groundwater level and quality in the Baotu Spring area of Jinan City were quantitatively analyzed by multi-methods. This study focuses on temperate semi-arid fissured karst systems, proposing an integrated multi-method quantitative approach combining isotopic analysis, flow monitoring, tracer tests, and numerical modeling. The methodology was developed to investigate the impacts of managed aquifer recharge (MAR) and extraction on karst groundwater level and quality dynamics, with a case study conducted in the Baotu Spring karst system, Jinan, China.

The main conclusions are summarized as follows: (1) The conventional two-endmember mixing

The main conclusions are summarized as follows: (1) The conventional two-endmember mixing model for recharge estimation was enhanced by integrating δ^2H (%) and $\delta^{18}O$ (%) data from both surface water and groundwater, which reduced uncertainties in estimating groundwater recharge ratios from

Commented [HC2]: This figure has been modified, with the original 9 subfigures reduced to 4, while the remaining ones have been moved to Supplement Material. multiple sources. The calculated mixing ratios of groundwater recharge indicate that surface water accounts for over 80% and 50% of groundwater recharge near the MAR segments of Yufu River and Xingji River, respectively. Firstly, the δ²H‰ and δ¹⁸O‰ values of groundwater and surface water reveals that surface water is an essential source of groundwater recharge and plays a crucial role in maintaining groundwater volume. In the southern metamorphic rock and Cambrian Zhangxia Formation limestone outcrop areas, as well as the northwestern Yellow River alluvial plain, the surface water recharge proportion is generally less than 20%. Near the MAR segments of the Yufu River and Xingji River, the mixing percentage of surface water recharge exceed 80% and 50%, respectively. (2) The relationship between effective MAR rates and water release rates was quantified through flow monitoring and infiltration tests, thereby improving recharge rate quantification accuracy. Results indicate that when water release rates surpass a critical threshold (20.44×104 m³/d for Yufu River and 2×10⁴ m³/d for Xingji River), partial surface water flows downstream, diminishing the effective MAR rate. (3) Based on large-scale regional tracer tests, Secondly, the analysis of the rivers' flow monitoring results reveals that some surface water will flow out downstream when the water release rate of the Yufu River and Xingji River exceeds 20.44×10⁴m³/d and 2×10⁴m³/d, respectively, reducing the actual MAR rate. However, according to the analysis of the infiltration test results, the theoretical maximum recharge capacity of the Yufu River to karst groundwater is about $114.9 \times 10^4 \text{m}^3 / \text{d}$. the effective porosity of the investigated karst aquifer was estimated to be approximately 1.08×10⁻⁴, which enhances the reliability of solute transport simulations. This value is comparable to results reported from similar karst terrains in Europe. (4) Thirdly, the isoline map of tracer peak concentration diffusion estimated the effective porosity of the karst aquifer in the study area to be 1.08 × 10-4, providing a

729

730

731

732

733

734

735

736

737

738

739

740

741

742

743

744

745

746

747

748

749

750

reference for solute transport modeling in similar hydrogeological conditions. According to the

simulations of the groundwater flow model, MAR effectively raises karst groundwater levels, and the effectiveness varies for the three MAR sources. MAR in wells has the best effect and fastest response, followed by the MAR in Xingji River, though both have low maximum recharge capacities. The MAR from Yufu River has a lower effect but the highest maximum recharge capacity. Furthermore, transferring some amount of the groundwater exploitation from eastern suburbs wells to western suburbs wells might reduce the impact on the water level of Baotu Spring. Using image data from exposed fissures to measure apertures, a maximum Reynolds number (Re≈2.24) for karst groundwater flow was calculated, confirming laminar flow conditions and validating the EPM model's applicability for the studied karst system. (5) Groundwater flow and solute transport modeling was employed to assess the effects of MAR and extraction on groundwater levels and quality. The results indicate that MAR significantly raises karst groundwater levels, though efficiency varies by different MAR sources. Prolonged recharge with poor-quality MAR water may degrade groundwater quality, and the maximum allowable sulfate concentrations in MAR water to meet China's Class I, II, and III groundwater standards are 56.5 mg/L, 197.8 mg/L, and 339.1 mg/L, respectively. Finally, poor quality of MAR water would negatively affect karst groundwater, and there is a linear relationship between the concentration of hydrochemical component in MAR water and karst groundwater, allowing for the pre-setting of karst groundwater quality targets and the determination of minimum standards for MAR water quality based on this relationship. Overall, the methodology proposed in this study effectively analyzes the impacts of MAR and extraction on groundwater level and quality. The integrated approach leverages multi-source data to achieve quantitative results. These findings provide a reference for MAR implementation in temperate semi-arid fissured karst systems with hydrogeological conditions similar to the Baotu Spring area.

751

752

753

754

755

756

757

758

759

760

761

762

763

764

765

766

767

768

769

770

771

773	In summary, the MAR projects in the Baotu Spring area of Jinan City have significantly impacted
774	the dynamics of karst groundwater level and quality. Proper planning and monitoring of the amount and
775	quality of MAR and groundwater exploitation are essential for maintaining groundwater levels, ensuring
776	continuous spring flow, and safeguarding groundwater quality.
777	Statements and Declarations
778	Data availability
779	The data underlying this article were provided by 801 Institute of Hydrogeology and Engineering
780	Geology, Shandong Provincial Bureau of Geology & Mineral Resources by permission. Data will be
781	shared on request to the corresponding author with permission.
782	Author Contribution
783	The respective contributions of all authors to this paper are as follows:
784	Cao H.: Conceptualization, Methodology, Writing-Original Draft.
785	Dong W. H.: Writing-Review and Editing, Supervision, Project administration.
786	Hu C. P., Chen H. L.: Resources, Funding acquisition, Investigation, Data Curation.
787	Qian J. L.: Investigation, Data Curation.
788	Liu C. W., Lyu M. H., Gao S.: Resources, Funding acquisition.
789	Competing Interests
790	The authors have no relevant financial or non-financial interests to disclose.
791	Acknowledgments
792	Many thanks to the sponsoring organizations (801 Institute of Hydrogeology and Engineering
793	Geology, Shandong Provincial Bureau of Geology & Mineral Resources) that made this research possible
794	Financial support
795	This manuscript was funded by National Key Research and Development Program (No

- 796 2024YFC3713100), National Natural Science Foundation of China (42202294) and Shandong Provincial
- 797 Natural Science Foundation (ZR2021QD084)The authors declare that no funds, grants, or other support
- 798 were received during the preparation of this manuscript.

References

- Aeschbach-Hertig, W., & Gleeson, T. (2012). Regional strategies for the accelerating global problem of groundwater depletion. *Nature Geoscience*, *5*(12), 853-861. https://doi.org/10.1038/ngeo1617
- Agbotui, P. Y., West, L. J., & Bottrell, S. H. (2020). Characterisation of fractured carbonate aquifers using ambient borehole dilution tests. *Journal of Hydrology*, 589. https://doi.org/10.1016/j.jhydrol.2020.125191
- Ajjur, S. B., & Baalousha, H. M. (2021). A review on implementing managed aquifer recharge in the Middle East and North Africa region: methods, progress and challenges. *Water International*, 46(4), 578-604. https://doi.org/10.1080/02508060.2021.1889192
- Akurugu, B. A., Obuobie, E., Yidana, S. M., Stisen, S., Seidenfaden, I. K., & Chegbeleh, L. P. (2022).
 Groundwater resources assessment in the Densu Basin: A review. *Journal of Hydrology: Regional Studies*, 40. https://doi.org/10.1016/j.ejrh.2022.101017
- Alam, S., Borthakur, A., Ravi, S., Gebremichael, M., & Mohanty, S. K. (2021). Managed aquifer
 recharge implementation criteria to achieve water sustainability. *Sci Total Environ*, 768, 144992.
 https://doi.org/10.1016/j.scitotenv.2021.144992
- Aliouache, M., & Jourde, H. (2024). Influence of structural properties and connectivity of initial fracture network on incipient karst genesis. *Journal of Hydrology*, 640. https://doi.org/10.1016/j.jhydrol.2024.131684
- Allocca, V., Manna, F., & De Vita, P. (2014). Estimating annual groundwater recharge coefficient for
 karst aquifers of the southern Apennines (Italy). Hydrology and Earth System Sciences, 18(2),
 803-817. https://doi.org/10.5194/hess-18-803-2014
- 820 Bakalowicz, M. (2005). Karst groundwater: a challenge for new resources. *Hydrogeology Journal*, *13*(1), 821 148-160. https://doi.org/10.1007/s10040-004-0402-9
- Ballesteros, D., Farrant, A., Nehme, C., Woods, M., Todisco, D., & Mouralis, D. (2020). Stratigraphical
 influence on chalk cave development in Upper Normandy, France: implications for chalk
 hydrogeology. *International Journal of Speleology*, 49(3), 187-208.
 https://doi.org/10.5038/1827-806x.49.3.2319
- Bhering, A. P., Antunes, I. M. H. R., Marques, E. A. G., & de Paula, R. S. (2021). Geological and hydrogeological review of a semi-arid region with conflicts to water availability (southeastern Brazil). *Environmental Research*, 202. https://doi.org/10.1016/j.envres.2021.111756
- Cao, H., Dong, W., Chen, H., & Wang, R. (2023). Groundwater vulnerability assessment of typical
 covered karst areas in northern China based on an improved COPK method. *Journal of Hydrology*, 624. https://doi.org/10.1016/j.jhydrol.2023.129904
- Cao, X., Zhang, J., Meng, H., Lai, Y., & Xu, M. (2023). Remote sensing inversion of water quality parameters in the Yellow River Delta. *Ecological Indicators*, 155. https://doi.org/10.1016/j.ecolind.2023.110914
- Chang, Y., Wu, J., & Liu, L. (2015). Effects of the conduit network on the spring hydrograph of the karst

- 836 aquifer. Journal of Hydrology, 527, 517-530. https://doi.org/10.1016/j.jhydrol.2015.05.006
- 837 Craig, H. (1961). Isotopic Variations in Meteoric Waters. *Science (New York, N.Y.)*, *133*(3465), 1702-838 1703. https://doi.org/10.1126/science.133.3465.1702
- 839 Criss, R. E. (2010). A DARCIAN MODEL FOR THE FLOW OF BIG SPRING AND THE 840 HYDRAULIC HEAD IN THE OZARK AQUIFER, MISSOURI, USA. *Acta Carsologica*, 841 39(2), 379-387. <Go to ISI>://WOS:000281922700016
- Daher, W., Pistre, S., Kneppers, A., Bakalowicz, M., & Najem, W. (2011). Karst and artificial recharge:

 Theoretical and practical problems. *Journal of Hydrology*, 408(3-4), 189-202.

 https://doi.org/10.1016/j.jhydrol.2011.07.017
- Deng, X., Xing, L., Yu, M., Zhao, Z., Li, C., & Su, Q. (2022). Characteristics of the water cycle of Jinan
 karst spring in northern China. Water Practice and Technology, 17(7), 1470-1489.
 https://doi.org/10.2166/wpt.2022.075
- Foley, A., Cachandt, G., Franklin, J., Willmore, F., & Atkinson, T. (2012). Tracer tests and the structure of permeability in the Corallian limestone aquifer of northern England, UK. *Hydrogeology Journal*, 20(3), 483-498. https://doi.org/10.1007/s10040-012-0830-x
- Foley, J. A., Ramankutty, N., Brauman, K. A., Cassidy, E. S., Gerber, J. S., Johnston, M., Mueller, N.
 D., O'Connell, C., Ray, D. K., West, P. C., Balzer, C., Bennett, E. M., Carpenter, S. R., Hill, J.,
 Monfreda, C., Polasky, S., Rockstrom, J., Sheehan, J., Siebert, S., Tilman, D., & Zaks, D. P.
 (2011). Solutions for a cultivated planet. *Nature*, 478(7369), 337-342.
 https://doi.org/10.1038/nature10452
- Gao, M., Li, X., Qian, J., Wang, Z., Hou, X., Gui, C., Bai, Z., Fu, C., Li, J., & Zuo, X. (2023).
 Hydrochemical Characteristics and Controlling Factors of Shallow and Deep Groundwater in
 the Heilongdong Spring Basin, Northern China. Sustainability, 15(21).
 https://doi.org/10.3390/su152115447
- Gao, S., Li, C., Liu, Y., Sun, B., Zhao, Z., Lv, M., & Gang, S. (2023). Hydrogeochemical Characteristics
 and Evolution Processes of Karst Groundwater Affected by Multiple Influencing Factors in a
 Karst Spring Basin, Eastern China. Water, 15(22). https://doi.org/10.3390/w15223899
- Guo, Y., Qin, D., Li, L., Sun, J., Li, F., & Huang, J. (2019). A Complicated Karst Spring System:
 Identified by Karst Springs Using Water Level, Hydrogeochemical, and Isotopic Data in Jinan,
 China. Water, 11(5). https://doi.org/10.3390/w11050947
- Hartmann, A., Gleeson, T., Rosolem, R., Pianosi, F., Wada, Y., & Wagener, T. (2015). A large-scale
 simulation model to assess karstic groundwater recharge over Europe and the Mediterranean.
 Geoscientific Model Development, 8(6), 1729-1746. https://doi.org/10.5194/gmd-8-1729-2015
- Hartmann, A., Goldscheider, N., Wagener, T., Lange, J., & Weiler, M. (2014). Karst water resources in
 a changing world: Review of hydrological modeling approaches. *Reviews of Geophysics*, 52(3),
 218-242. https://doi.org/10.1002/2013rg000443
- Jiang, C., Wang, X., Pu, S., & Jourde, H. (2022). Incipient karst generation in jointed layered carbonates:
 Insights from three-dimensional hydro-chemical simulations. *Journal of Hydrology*, 610.
 https://doi.org/10.1016/j.jhydrol.2022.127831
- Jiang, X., Lei, M., & Zhao, H. (2019). Review of the advanced monitoring technology of groundwater–
 air pressure (enclosed potentiometric) for karst collapse studies. *Environmental Earth Sciences*,
 78(24). https://doi.org/10.1007/s12665-019-8716-z
- Jourde, H., & Wang, X. (2023). Advances, challenges and perspective in modelling the functioning of karst systems: a review. Environmental Earth Sciences, 82(17). https://doi.org/10.1007/s12665-

- 880 <u>023-11034-7</u>
- Kang, F., Jin, M., & Qin, P. (2011). Sustainable yield of a karst aquifer system: a case study of Jinan
 springs in northern China. *Hydrogeology Journal*, 19(4), 851-863.
 https://doi.org/10.1007/s10040-011-0725-2
- Kidmose, J., Nilsson, B., Klem, N. K., Pedersen, P. G., Henriksen, H. J., & Sonnenborg, T. O. (2023).
 Can effective porosity be used to estimate near-well protection zones in fractured chalk?
 Hydrogeology Journal, 31(8), 2197-2212. https://doi.org/10.1007/s10040-023-02743-1
- Knöll, P., & Scheytt, T. (2017). A tracer test to determine a hydraulic connection between the Lauchert
 and Danube karst catchments (Swabian Alb, Germany). *Hydrogeology Journal*, 26(2), 429-437.
 https://doi.org/10.1007/s10040-017-1678-x
- Li, J., Wang, W., & Li, W. (2023). Total Dissolved Solids Risk Assessment and Optimisation Scheme
 of Managed Aquifer Recharge Projects in a Karst Area of Northern China. Water, 15(22).
 https://doi.org/10.3390/w15223930
- Li, M., Liu, T., Duan, L., Luo, Y., Ma, L., Zhang, J., Zhou, Y., & Chen, Z. (2019). The Scale Effect of
 Double-Ring Infiltration and Soil Infiltration Zoning in a Semi-Arid Steppe. Water, 11(7).
 https://doi.org/10.3390/w11071457
- Li, M., Xie, Y., Dong, Y., Wang, L., & Zhang, Z. (2023). Review: Recent progress on groundwater
 recharge research in arid and semiarid areas of China. *Hydrogeology Journal*, 32(1), 9-30.
 https://doi.org/10.1007/s10040-023-02656-z
- Li, T., Zhang, J., Gao, Y., Cao, X., Liu, H., Zhang, P., Yang, J., & Mastrocicco, M. (2020). Hydrological
 Characteristics of Ordovician Karst Top in a Deep Region and Evaluation of Its Threat to Coal
 Mining: A Case Study for the Weibei Coalfield in Shaanxi Province, China. *Geofluids*, 2020,
 1-17. https://doi.org/10.1155/2020/7629695
- Liang, Y., Gao, X., Zhao, C., Tang, C., Shen, H., Wang, Z., & Wang, Y. (2018). Review: Characterization,
 evolution, and environmental issues of karst water systems in Northern China. *Hydrogeology Journal*, 26(5), 1371-1385. https://doi.org/10.1007/s10040-018-1792-4
- Liu, C., Zhang, G., & Wang, W. (2021). Characteristics of an open karst water system in Shandong
 Province, China. Environmental Earth Sciences, 80(4). https://doi.org/10.1007/s12665-021-09465-1
- Liu, Y., Wang, M., Webber, M., Zhou, C., & Zhang, W. (2020). Alternative water supply solutions:
 China's South-to-North-water-diversion in Jinan. J Environ Manage, 276, 111337.
 https://doi.org/10.1016/j.jenvman.2020.111337
- Lorenzi, V., Banzato, F., Barberio, M. D., Goeppert, N., Goldscheider, N., Gori, F., Lacchini, A., Manetta,
 M., Medici, G., Rusi, S., & Petitta, M. (2024). Tracking flowpaths in a complex karst system
 through tracer test and hydrogeochemical monitoring: Implications for groundwater protection
 (Gran Sasso, Italy). Heliyon, 10(2), e24663. https://doi.org/10.1016/j.heliyon.2024.e24663
- Luo, Q., Yang, Y., Qian, J., Wang, X., Chang, X., Ma, L., Li, F., & Wu, J. (2020). Spring protection and
 sustainable management of groundwater resources in a spring field. *Journal of Hydrology*, 582.
 https://doi.org/10.1016/j.jhydrol.2019.124498
- 919 Medici, G., Munn, J. D., & Parker, B. L. (2024). Delineating aquitard characteristics within a Silurian 920 dolostone aquifer using high-density hydraulic head and fracture datasets. *Hydrogeology* 921 *Journal*, 32(6), 1663-1691. https://doi.org/10.1007/s10040-024-02824-9
- 922 Medici, G., Smeraglia, L., Torabi, A., & Botter, C. (2021). Review of Modeling Approaches to 923 Groundwater Flow in Deformed Carbonate Aquifers. *Ground Water*, 59(3), 334-351.

924 <u>https://doi.org/10.1111/gwat.13069</u>

944

945

- Medici, G., & West, L. J. (2021). Groundwater flow velocities in karst aquifers; importance of spatial
 observation scale and hydraulic testing for contaminant transport prediction. *Environ Sci Pollut Res Int*, 28(32), 43050-43063. https://doi.org/10.1007/s11356-021-14840-3
- 928 Medici, G., West, L. J., Chapman, P. J., & Banwart, S. A. (2019). Prediction of contaminant transport in 929 fractured carbonate aquifer types: a case study of the Permian Magnesian Limestone Group (NE 930 England, UK). Sci Pollut ResInt, 26(24), 24863-24884. Environ https://doi.org/10.1007/s11356-019-05525-z 931
- Mudarra, M., Hartmann, A., & Andreo, B. (2019). Combining Experimental Methods and Modeling to
 Quantify the Complex Recharge Behavior of Karst Aquifers. Water Resources Research, 55(2),
 1384-1404. https://doi.org/10.1029/2017wr021819
- Niu, S., Shu, L., Li, H., Xiang, H., Wang, X., Opoku, P. A., & Li, Y. (2021). Identification of Preferential
 Runoff Belts in Jinan Spring Basin Based on Hydrological Time-Series Correlation. *Water*,
 13(22). https://doi.org/10.3390/w13223255
- 938 Ostad-Ali-Askari, K., & Shayannejad, M. (2021). Quantity and quality modelling of groundwater to 939 manage water resources in Isfahan-Borkhar Aquifer. *Environment, Development and* 940 *Sustainability*, 23(11), 15943-15959. https://doi.org/10.1007/s10668-021-01323-1
- Pagnozzi, M., Coletta, G., Leone, G., Catani, V., Esposito, L., & Fiorillo, F. (2020). A Steady-State
 Model to Simulate Groundwater Flow in Unconfined Aquifer. *Applied Sciences*, 10(8).
 https://doi.org/10.3390/app10082708
 - Perrin, J., Parker, B. L., & Cherry, J. A. (2011). Assessing the flow regime in a contaminated fractured and karstic dolostone aquifer supplying municipal water. *Journal of Hydrology*, 400(3-4), 396-410. https://doi.org/10.1016/j.jhydrol.2011.01.055
- Ren, S., Gragg, S., Zhang, Y., Carr, B. J., & Yao, G. (2018). Borehole characterization of hydraulic
 properties and groundwater flow in a crystalline fractured aquifer of a headwater mountain
 watershed, Laramie Range, Wyoming. *Journal of Hydrology*, 561, 780-795.
 https://doi.org/10.1016/j.jhydrol.2018.04.048
- Ringleb, J., Sallwey, J., & Stefan, C. (2016). Assessment of Managed Aquifer Recharge through
 Modeling—A Review. Water, 8(12). https://doi.org/10.3390/w8120579
- Scanlon, B. R., Mace, R. E., Barrett, M. E., & Smith, B. (2003). Can we simulate regional groundwater
 flow in a karst system using equivalent porous media models? Case study, Barton Springs
 Edwards aquifer, USA. *Journal of Hydrology*, 276(1-4), 137-158.
 https://doi.org/10.1016/s0022-1694(03)00064-7
- Sherif, M., Sefelnasr, A., Al Rashed, M., Alshamsi, D., Zaidi, F. K., Alghafli, K., Baig, F., Al-Turbak,
 A., Alfaifi, H., Loni, O. A., Ahamed, M. B., & Ebraheem, A. A. (2023). A Review of Managed
 Aquifer Recharge Potential in the Middle East and North Africa Region with Examples from
 the Kingdom of Saudi Arabia and the United Arab Emirates. Water, 15(4).
 https://doi.org/10.3390/w15040742
- Standen, K., Costa, L. R. D., & Monteiro, J.-P. (2020). In-Channel Managed Aquifer Recharge: A
 Review of Current Development Worldwide and Future Potential in Europe. Water, 12(11).
 https://doi.org/10.3390/w12113099
- Wang, G.-F., Wu, Y.-X., Lu, L., Li, G., & Shen, J. S. (2017). Investigation of the geological and
 hydrogeological environment with relation to metro system construction in Jinan, China.
 Bulletin of Engineering Geology and the Environment, 78(2), 1005-1024.

- 968 https://doi.org/10.1007/s10064-017-1140-2
- Wang, W., Fan, Y., Li, K., Wang, X., & Kang, J. (2022). Challenges of Spring Protection and
 Groundwater Development in Urban Subway Construction: A Case Study in the Jinan Karst
 Area, China. Water, 14(9). https://doi.org/10.3390/w14091521
- Worthington, S. R. H., Foley, A. E., & Soley, R. W. N. (2019). Transient characteristics of effective
 porosity and specific yield in bedrock aquifers. *Journal of Hydrology*, 578.
 https://doi.org/10.1016/j.jhydrol.2019.124129
- Xanke, J., Liesch, T., Goeppert, N., Klinger, J., Gassen, N., & Goldscheider, N. (2017). Contamination
 risk and drinking water protection for a large-scale managed aquifer recharge site in a semi-arid
 karst region, Jordan. *Hydrogeology Journal*, 25(6), 1795-1809. https://doi.org/10.1007/s10040-017-1586-0
- Xi, H., Zhang, L., Feng, Q., Si, J., Chang, Z., Yu, T., & Li, J. (2015). The spatial heterogeneity of riverbed
 saturated permeability coefficient in the lower reaches of the Heihe River Basin, Northwest
 China. Hydrological Processes, 29(23), 4891-4907. https://doi.org/10.1002/hyp.10544
- Yin, L., Xu, B., Cai, W., Zhou, P., & Yang, L. (2023). Intrinsic Vulnerability Assessment of the Qingduo
 Karst System, Henan Province. Water, 15(19). https://doi.org/10.3390/w15193425
- Zafarmomen, N., Alizadeh, H., Bayat, M., Ehtiat, M., & Moradkhani, H. (2024). Assimilation of
 Sentinel-Based Leaf Area Index for Modeling Surface-Ground Water Interactions in Irrigation
 Districts. Water Resources Research, 60(10). https://doi.org/10.1029/2023wr036080
- Zhang, Z., & Nemcik, J. (2013). Fluid flow regimes and nonlinear flow characteristics in deformable
 rock fractures. *Journal of Hydrology*, 477, 139-151.
 https://doi.org/10.1016/j.jhydrol.2012.11.024
- Zhang, Z., & Wang, W. (2021). Managing aquifer recharge with multi-source water to realize sustainable
 management of groundwater resources in Jinan, China. Environ Sci Pollut Res Int, 28(9), 10872 10888. https://doi.org/10.1007/s11356-020-11353-3
- Zhang, Z., Xu, Y., Zhang, Y., & Cao, J. (2018). Review: karst springs in Shanxi, China. *Carbonates and Evaporites*, 34(4), 1213-1240. https://doi.org/10.1007/s13146-018-0440-3
- Zheng, Q. Y., Wang, W. P., Liu, S., & Qu, S. S. (2020). Physical clogging experiment of sand gravel infiltration with Yellow River water in the Yufuhe River channel of Jinan, China [Review].
 Frontiers of Earth Science, 14(2), 306-314. https://doi.org/10.1007/s11707-019-0772-x
- Zhu, H., Xing, L., Meng, Q., Xing, X., Peng, Y., Li, C., Li, H., & Yang, L. (2020). Water Recharge of
 Jinan Karst Springs, Shandong, China. Water, 12(3). https://doi.org/10.3390/w12030694
- Zimmerman, R. W., & Bodvarsson, G. S. (1996). Hydraulic conductivity of rock fractures. *Transport in Porous Media*, 23(1), 1-30. https://doi.org/10.1007/BF00145263
- Zuber, A., & Motyka, J. (1994). Matrix porosity as the most important parameter of fissured rocks for solute transport at large scales. *Journal of Hydrology*, *158*(1-2), 19-46. https://doi.org/10.1016/0022-1694(94)90044-2